C.P. No. 995

C.P. No. 995

MINISTRY OF TECHNOLOGY

AERONAUTICAL RESEARCH COUNCIL

CURRENT PAPERS

The Dynamic Stability Derivatives of a Slender Wing, a Comparison of Theory with Free-Flight Model Tests at Near-Zero Lift, M = 0.8 to 2.4

by

K. J. Turner, A. Jean Ross and Geraldine Earley

LONDON: HER MAJESTY'S STATIONERY OFFICE

1968

PRICE 13s 0d NET

U.D.C. No.533.6.013.417 : 533.693.3 : 533.6.011.34/5 : 533.6.072

C.P. No. 995*
June 1966

THE DYNAMIC STABILITY DERIVATIVES OF A SLENDER WING, A COMPARISON OF THEORY WITH FREE-FLIGHT MODEL TESTS AT NEAR-ZERO LIFT, M = 0.8 to 2.4

by

K. J. Turner
A. Jean Ross
Geraldine Earley

SUMMARY

Results are presented for the stability derivatives of a slender-wing and fin configuration as obtained from a series of tests with models flying at near-zero lift. These results are compared with theoretical estimates obtained from lifting surface theory at subsonic speeds and slender-wing and linearised supersonic theory at supersonic speeds. The agreement between the experimental and theoretical results is satisfactory, the largest discrepancies occurring at transonic speeds and at the higher supersonic Mach numbers.

---

* Replaces R.A.E. Technical Report No. 66170 - A.R.C. 28574

CONTENTS

ILLUSTRATIONS

ILLUSTRATIONS (Contd)

1 INTRODUCTION

Over the past few years a great deal of experimental and theoretical work has been done on the aerodynamics of slender wings[1], mainly directed towards the design of supersonic transport aircraft. While some of this information has been used in theoretical studies of the dynamic characteristics[2,3] of such aircraft, and experimental work[4] has been done at low speeds, little had, at the time of starting this investigation, been attemped for supersonic flight conditions. The slender-wing configuration raises many novel stability problems. For example, several of the lateral stability derivatives are strongly dependent on incidence so that pronounced aerodynamic coupling may arise between the longitudinal and lateral motions. Furthermore, the very small moment of inertia about the rolling axis compared with the moments of inertia about the other axes may result in very different lateral oscillatory characteristics from those of conventional subsonic aircraft.

For these reasons, quite apart from the general ones involved in the design of most aircraft, it is important that the stability derivatives be measured at transonic and supersonic speeds so that the characteristics of any particular slender-wing design can be accurately calculated. The measured derivatives may also be used to check the validity of present theoretical methods[5] of estimation, extending the comparisons already made for subsonic conditions[6], and enabling estimates to be made for the derivatives of other similar slender-wing designs. Standard wind-tunnel techniques can, of course, yield data on all the longitudinal and lateral static stability derivatives, and their variation with incidence. The measurement of the rotary and acceleration derivatives is more difficult, although Thompson and Fail[7] have evolved a wind-tunnel technique using oscillating models throughout the speed range. However, at the time this investigation started, the only feasible way of obtaining the required information was by the free-flight model technique, and so a series of tests with rocket-boosted models was made and the results are reported here. The derivatives are obtained under oscillatory conditions, and results are given for derivatives due to incidence and sideslip (corresponding to the static derivatives measured under steady conditions in the tunnel tests), and for most of the more important derivatives due to angular velocities. An additional advantage of this method is that the models are completely unrestrained, so that any unexpected flight characteristic (e.g. an autorotational state) can be observed and investigated.

In order to facilitate the desired comparison between experimental and theoretical results a planform was chosen which is typical of a range of configurations studied for the supersonic transport but at the same time is simple enough to be amenable to theoretical treatment.

The eventual aim of the programme is to measure and compare the derivatives over a range of lifting conditions so that the lift-dependent effects can be studied. The present paper is concerned with the necessary first stage of obtaining the derivatives at zero lift. In flying the models, however, it is not possible to obtain precisely zero-lift conditions at all times and so some lifting effects are included. For the theoretical estimation of the derivatives, the effects of leading edge vortices are neglected at supersonic speeds, so that "classical" linearised theories may be used for the wing and fin contributions. Interference effects between the wing and fin are estimated, usually on the basis of slender body theory, and the increments due to wing thickness are included.

The experimental technique depended on exciting either the short-period pitching oscillation or the lateral Dutch-roll oscillation by disturbing the model during its flight by firing small pulse-rockets. Before the model design was finally settled, some preliminary theoretical studies were made on a Short's analogue computer. These gave a valuable insight into the relative magnitudes and types of response that could be induced by firing sets of pulse rockets in various ways to produce different combinations of pitching moment, rolling moment, yawing moment, normal force and side force. The effects of some of the aerodynamic cross-coupling derivatives were also explored in this way.

In this programme the experimental technique was being developed and new kinds of instruments were being tried and developed, and so a relatively large number of models had to be flown to collect data of the required quantity and quality. The experimental results have, in fact, been compiled from the flight records of eight models.

Three specialised test-vehicles, for measuring the roll damping derivative under steady-state conditions[8], were also flown. From these tests results are presented for wings of different stiffness and for the incremental effect of a dorsal fin.

2 EXPERIMENTAL TECHNIQUE

2.1 Design of models

The model design is illustrated in Figs.1 to 4, and the main data are given in Table 1. The wing planform is delta-type, with parabolic tips, (Fig.1), and with thickness distribution such that the spanwise section is diamond, and the chordwise section, on the centreline, parabolic. The fin is of similar planform, but with less leading edge sweep, and has flat chordwise sections, although a few of the early models had a cropped delta fin of the same area and sweepback.

Because of the very simple configuration chosen for this investigation a cheap and rapid method of model construction could be adopted. In the event, the relative cheapness of the models allowed a large number of them to be made and flown for a number of investigations additional to these experiments on dynamic stability.

The method of construction was common to all the models although their internal equipment differed considerably. The wing was constructed as a sandwich having a $\frac{1}{4}$-inch-thick aluminium alloy centre-plate forming the wing planform, and hence the leading and trailing edges, with hollow glass fibre mouldings glued above and below to provide the profile shape (Fig.2(a) and (c)). These were moulded to the required dimensions and finish on the outer surface so that no hand working was required over the larger part of the wing. Inside the mouldings a number of spanwise and chordwise stiffening ribs were incorporated which were also bonded to the centre-plate. The early models in the series had only four chordwise ribs and experienced a violent vibration in several different modes at Mach numbers above 1.7. For the free-flight stability investigation this vibration had to be restrained or avoided because it ruined the telemetry transmission and compromised the aerodynamic conditions of the test. It was found that increasing the number of chordwise ribs progressively raised the Mach number at which the vibration started and eventually an arrangement of 14 ribs, shown in Fig.2(c), was chosen because it eliminated the most troublesome vibration modes at Mach numbers below 2.1.

The fin was a hollow structure fabricated from aluminium alloy sheet and was bolted along its base to the wing centre-plate. The fin section was flat, with a blunt trailing edge and the front 8% of the chord was rounded off to a circular-arc section to give a sharp leading edge and a tangential junction with the flat portion of section.

Detachable hatches were provided in the top surface of the wing to give access to the instrumentation and pulse-rocket installations (Fig.2(b)). The recess in the underside of the model, for the boost-motor attachment hook, was covered by a retractable door to preserve the shape of the wing profile but the ports for the pulse-rocket nozzles had to be left uncovered. Two pyrotechnic flares were faired into the underside of the wing at the trailing-edge centre-line. These were required to assist the operators of the visual-tracking equipment at the range.

Each model was ballasted to bring the centre of gravity as close as possible to the desired mid-point of the centre-line chord. This was achieved within the limits -0.01 to +0.04 c_o for all the models in the series. No attempt was made to give all the models the same inertia characteristics but the moments of inertia of each model were measured and incorporated in the analysis of the results.

The method adopted for disturbing the models in flight was to fire the pulse rockets by a clockwork sequence switch at pre-determined times. The array of pulse rockets used on the later models in the series is shown in Fig.3(a). Early models had either the set of eight pulse rockets at the mid-chord for lateral stability tests or the set of twelve at the rear for longitudinal stability tests. On the basis of some theoretical studies made on an analogue computer the pulse rockets were chosen to give a thrust of 180 lb for 0.07 seconds duration and were arranged to fire in pairs. The pulse rockets at the mid-chord were fired in opposed pairs so that a pure rolling couple was produced with no resultant normal force, assuming perfect matching of the pair. The pulse rockets at the rear were fired either as a symmetrical pair about the centre line to produce a combined pitching moment and normal force with no lateral component or as an asymmetric pair on one side of the fin. The latter arrangement produced a pitching moment and normal force but the dominant effect was to provide a large yawing moment plus side force arising from the shock-induced loading on one side of the fin.

2.2 Instrumentation

All the models were equipped with the R.A.E. 465 Mc/s sub-miniature telemetry system but there were considerable differences between the instrumentation details adopted for the various models. For example some carried two multi-channel sets to provide a large capacity for data transmission, some carried one multi-channel set and a Doppler transponder system for improved trajectory determination and some carried one telemetry set only. In all cases the aerials were either mounted flush with the wing surface or behind the blunt trailing edge of the fin so that the shape of the models was unaffected from the aerodynamic point of view.

There was also considerable variation in the choice and arrangement of the transducers for the various models. This was largely dictated by the specific purpose for which a given model was to be flown but it also arose in the search for an adequate method of measuring the rotary components of motion, which is an essential requirement of the analysis procedure. In the course of the tests three methods were used,

(a) rate gyroscopes

(b) displaced and differenced linear accelerometers

(c) angular accelerometers.

On several of the models two of these methods were used simultaneously. A typical arrangement of transducers as used on the later and most successful models is shown in Fig.3(b). Most of the measurements were made by differencing pairs of linear accelerometers. The differencing was not done electrically within the model but subsequently during the analysis in order to obtain the highest degree of reliability and accuracy. This method was entirely satisfactory for determining the angular accelerations in pitch and yaw but was not so good for the roll acceleration because the accelerometers could not be placed sufficiently far apart (Fig.3(b)). In principle, rate gyroscopes are a satisfactory way of measuring the rotary motion but they suffered the following disadvantages in practice:-

(a) their power supplies required a relatively heavy rotary convertor having an inevitable gyroscopic couple,

(b) the roll gyro was sensitive to any steady rate of roll performed by the model as well as to the oscillatory component to be measured, (this was, at times, a large effect),

(c) the yaw gyro was sensitive to the rate of curvature of the flight path whenever the model was flying with its wings out of the horizontal, this usually being a small effect.

A more preferable instrument, which avoids these difficulties, is the angular accelerometer. The only suitable instrument of this kind readily available was a spring-mass transducer with a variable capacity output that had been developed, but not used, by Space Department, R.A.E. Inevitably a number of practical difficulties arose in using this untried instrument but it eventually proved to be the best method of obtaining the required measurements. It was used for the rolling axis only since the displaced linear accelerometers were satisfactory for the other axes.

2.3 Flight tests

The models were launched pick-a-back fashion from solid-fuel rocket motors (Fig.4(a)). Two sizes of rocket motor were used depending on whether the maximum Mach number was to be about M = 2 or M = 1.3. The larger motor was potentially able to accelerate the models to M = 2.5 but velocities above M = 2 were avoided for the later models because of the flutter problem already mentioned.

The vehicles were launched on a fairly low trajectory in order to obtain the maximum Reynolds number and the highest possible quality of experimental data. Typically the maximum altitude was about 5000 ft and the range about 50000 ft. During the coasting portion of the flight, while the stability tests were being made, the models were, of course, free to roll and trim according to any imperfections in their shape. They generally performed a steady roll, to port or starboard, of about 50° per second which is low enough to have a negligible effect on the dynamics of the superimposed oscillatory motions. The trim conditions varied somewhat from model to model. At Mach numbers above 1.4 they generally flew at very nearly zero lift, but as the Mach numbers fell to near sonic the trim usually changed rather quickly to a small negative lift but sometimes to a small positive lift.

2.4 The roll-damping test vehicles

Supplementary to the main experimental investigation three special tests were made to measure the roll-damping derivative ℓ_p. The models were made of solid metal to one quarter scale of the external linear dimensions of the main models, and were attached to the nose of a test vehicle equipped with a roll balance. The whole vehicle was made to roll at a high rate so that the roll-damping component on the model could be measured directly by the roll balance. A photograph of one of the vehicles is shown in Fig.4(b).

Three kinds of model were used,

(1) the wing alone made in light alloy,

(2) the wing alone made in steel,

(3) the wing plus fins above and below (for symmetry) made in light alloy.

A comparison of the results from models (1) and (2) was intended to show the influence of aeroelastic distortion, and the difference between the results of models (1) and (3) yields the contribution of the fin to the total damping of the complete configuration.

On all the models the wings were of the same section and planform as in the stability models but a small modification had to be made at the rear to accommodate the sting mounting of the roll-balance.

3 ANALYSIS OF THE EXPERIMENTAL DATA

3.1 Basic data

Typical values of Reynolds number, and trimmed lift coefficient and approximate angle of incidence throughout the Mach number range are shown in Figs.5 and 6, together with the extent of variation between all the models.

An almost complete telemetry record from one of the models is reproduced in Fig.7. This particular form of presentation is used for visual assessment only and is not of sufficient accuracy for numerical analysis, for which the data was obtained either from the film record, or on later models in digital form recorded on magnetic tape. It does, however, conveniently show many interesting features of the model behaviour. When the model separates from its boost motor, at 3.8 seconds, it experiences disturbances in pitch and yaw which may be analysed to yield useful stability data. During the coasting part of the flight considerable differences can be seen in the types of response from firing different combinations of pulse rockets.

(a) When a rolling couple pair near the c.g. are fired there is very little response in pitch, e.g. at 7.4 seconds.

(b) When a symmetrical pair at the rear are fired there is very little response in yaw or roll, e.g. at 15 and 18.2 seconds.

(c) When an asymmetric pair adjacent to the fin are fired there is a very large response in yaw and roll with a moderate response in pitch, e.g. at 5.8, 8.7, 10.2 and 11.8 seconds.

On several of the lateral oscillations the roll subsidence mode can be observed superimposed on the roll record (e.g. at 10.2 and 11.8 seconds) and at

13.4 seconds the roll subsidence mode is dominant with the oscillatory mode almost completely absent. The significance of this is discussed later on. On this particular model the record from the angular accelerometer shows a certain amount of "fuzziness" during some of the oscillations. This was probably caused by vibration, in the rolling plane, of the instrument mounting bracket. Subsequent laboratory tests on an identical mounting showed that the degree of fuzziness could be accounted for by a vibration amplitude of only 0.00007 inches. Later models with a redesigned bracket showed no sign of this effect.

3.2 Longitudinal stability

The analysis of the longitudinal stability information was limited to evaluating the derivatives z_w, m_w and the damping pair $m_q + m_{\dot{w}}$. Standard methods of data reduction were used[9] based on an analysis of the frequency, damping and "focal point" of the short-period oscillation.

The longitudinal response is, of course, affected when there is also a significant response in the lateral modes, e.g. the oscillation starting at 10.2 and 11.8 seconds in Fig.7. Distortion of the damped harmonic wave form of the records of normal acceleration can be seen with the naked eye and the results from the "coupled" oscillations have not been included in this report.

The frequency of the longitudinal oscillation is shown in Fig.8(a) for the various models, and the reduced frequency of one model, 17, is seen to be between 0.112 and 0.115, Fig.8(b). The total damping, Fig.9(a), exhibits greater scatter than the frequency, but the variation with Mach number is clearly defined. Some results for $M > 2$ are also given, as some of the models were free of the flutter phenomenon at the speed of separation from the boost rocket.

3.3 Lateral stability

The motion in the lateral Dutch-roll mode is strongly affected by any motion in the longitudinal mode because of the large incidence-dependent derivatives on a configuration of this kind. In the present tests, however, it was possible to avoid such effects because the longitudinal motion damped out so much more quickly than the lateral motion, e.g. at 8.7, 10.2 and 11.8 seconds in Fig.7. The analysis of the lateral motion was therefore restricted to those parts of the flight record where the longitudinal motion had decayed to a negligibly small amplitude.

As already mentioned, the response to a lateral disturbance sometimes contained a significant contribution from the roll subsidence mode, so that

responses of the form $Ae^{-kt} + Be^{-\lambda_2 t} \sin(\nu_2 t + \varepsilon)$ had to be analysed. In order to separate the modes, successively corrected values of $A_1 e^{-k_1 t}$ were subtracted from the response until the peak values of the resultant oscillation lay on a straight line when plotted logarithmically. The final value of $k_1 (=k)$ obtained was used to determine an approximate value of the damping in roll derivative, ℓ_p.

The frequency of the Dutch-roll oscillation is shown in Figs.8(c) and (d), and the results for the various models are seen to be consistent. The total damping, Fig.9(b), exhibits a similar percentage scatter to that of the longitudinal oscillation, although the damping is smaller, as is to be expected for a slender wing design. The roll-subsidence damping, as obtained for one of the models, is shown in Fig.10.

The main method adopted for deriving the stability derivatives from the oscillatory mode was the time-vector solution developed by Doetsch[10]. A detailed description of how this technique is applied to free-flight model tests is given in Ref.11. Briefly, the amplitude and phase relationships, plotted in Figs.11(a) and 11(b), between the three degrees of freedom v, p, r, of the Dutch-roll oscillation are measured and used in vector solution for the rolling-moment and yawing-moment equations. Examples of the vector diagrams are shown in Figs.12(a) to (c). Measured values of the inertia characteristics are used and, in order to solve the two equations, one of the derivatives in each must be assumed. In the present case, estimated values of ℓ_r and n_p were used (Figs.13 and 14) because they are the least important ones, and the vector solution for the yawing moment equation has been obtained by neglecting the derivative n_v. However, the vector diagram (Fig.12(c)) of the kinematic equation

$$a_y \simeq \frac{V}{g}(\dot{\beta} + r)$$

shows that $\beta \simeq -r$, and so

$$\left(-n_r \frac{rb}{2V} - n_v \frac{\beta b}{2V}\right) \simeq (-n_r + n_v) \frac{rb}{2V} \quad .$$

Thus the vector labelled $(-n_r\ rb/2V)$ in Fig.12(a) may be taken to provide an approximate solution for the derivative pair $(n_r - n_v)$, and so the results have been presented this way.

In addition to the vector method the following analytic solutions were used to reduce some of the experimental data as a semi-independent check.

$$n_v \simeq \frac{i_z}{\mu_2} (\omega_2 \hat{t})^2 + \ell_v e_x \qquad (1)$$

$$y_v \simeq \frac{g \hat{t}}{V} R_{a_y \beta} \qquad (2)$$

$$\ell_v \simeq \frac{i_x}{\mu_2} (\hat{t} R_{r\beta})^2 \{R_{pr} + e_x\}/(1 - e_x e_z) \qquad (3)$$

While most of the perturbation parameters behave in an orderly manner over the Mach number range the behaviour of the roll/yaw amplitude ratio and phase angle (Fig.11) merits further comment. Between M = 1.25 and 1.4 there is a sudden phase-change of about 160 degrees accompanied by a translation through zero* of the amplitude ratio at M = 1.34 (i.e. at 14 seconds on the telemetry record Fig.7). This represents a de-coupling of the roll and yaw motions and probably explains why the pulse rocket at 13.4 seconds (on the model from which the record of Fig.7 was obtained) produced a roll subsidence mode only. In terms of the aerodynamic derivatives this behaviour is accounted for by a change of sign of the rolling moment due to sideslip derivative ℓ_v, due to interference between the fin and wing. The effect of this change in ℓ_v on the vector diagrams is illustrated in Fig.12. It is worth noting that the experimental points covering this particular feature of the results came from four models. Two yielded results from M = 1.8 down to 1.5, one yielded the points at M = 1.15 and 1.06 and the fourth covered the range from M = 1.8 down to 1.2. Although these four models did not fly at precisely the same trim conditions they were sufficiently similar for a valid comparison to be made.

Most of the values of ℓ_v plotted in Fig.21(a), including the sign change, were checked by equation (3), the results agreeing within 0.0005 ℓ_v in each case.

The experimental values of ℓ_p derived from both the oscillatory and roll-subsidence modes are plotted together in Fig.22(a). It is perhaps surprising, but encouraging, to observe that both kinds of analysis yield very similar results. The points showing the sudden reduction in ℓ_p below M = 1.25 came

---

* In the bottom diagram of Fig.11(a), the amplitude ratio R_{pr} is plotted above or below the zero magnitude axis according as ϕ_{pr} is less than or greater than 180°, in order to demonstrate the zero amplitude more clearly.

from two different models and so there is some confirmation that it is a genuine effect.

3.4 Steady-state roll damping

The results from the three roll-damping test vehicles (Fig.4(b)) are shown in Fig.22(b) and (c). The particular merit of this technique is that a continuous measurement of the roll-damping moment is obtained over the whole Mach number range, instead of at rather widely spaced discrete points as in the case of the stability models. Thus any sudden change of rolling moment over a small increment in Mach number, as might occur transonically, can be detected. It is clear that this has in fact happened, although in different ways, on all three models between M = 1.05 and 1.15.

The roll-damping moment obtained by this technique is, of course, measured under very different conditions from those on the stability models. Here a steady-state rolling motion is maintained, with a tip-helix angle of between 0.5 and 2.0 degrees whereas the rolling motion of the stability models is dynamic (whether oscillating, decaying or both) with a maximum tip-helix angle of about 0.02 degrees.

Nevertheless the general level of results, above M = 1.4, is very similar from both kinds of model. Below M = 1.25 the steady-state results do not show the sudden falling away that is an unexpected feature of the dynamic results.

Comparing the results from the two roll-damping models of different stiffness (models 1 and 2, Fig.23(b)) it is evident that there can be very little loss of roll-damping from aeroelastic distortion, bearing in mind that the steel model has three times the stiffness of the aluminium-alloy model. What difference there is between the two results can be accounted for by experimental uncertainties. In fact, between M = 1.2 and 1.9, the more flexible model shows the higher damping. This is impossible for such a planform where aeroelastic distortion at the tips causes the load to be shed and not increased. Therefore a mean line between the results from models 1 and 2 has been taken as representing the roll-damping derivative for the case of the wing alone.

Comparing the results from the models with and without the vertical fins, (Fig.22) shows that the fin contribution to ℓ_p is very small, as one might expect. Here one must remember that model 3 had vertical fins above and below the wing instead of on the upper surface only as on the stability models.

An interesting peculiarity is that all three models show quite different characteristics between M = 1.05 and 1.15. The models without fins show a 10% increase in damping, the steel one having a much more violent change, whereas the model with fins shows a decrease in damping of about 7%.

3.5 Accuracy

A general analysis of the accuracy with which the main flight parameters such as velocity, Mach number, dynamic pressure etc. can be established in free-flight model tests has been made by Picken[12]. Typical values are, velocity and Mach number 0.5%, dynamic pressure 1%.

The accuracy with which the aerodynamic derivatives can be determined from the stability models varies considerably from model to model, depending on the quality of the instrumentation and the amplitudes of the oscillations. Furthermore the accuracy with which different derivatives can be determined varies according to whether they have a dominant or minor influence on the motion. Thus m_w and n_v can generally be extracted to within about ±5% because they are the main stiffness terms in the longitudinal and lateral modes and so have the largest effect on the frequencies of the oscillations. On the other hand the yaw-damping derivative n_r has a relatively minor part to play and can be determined only within about ±20%. An immediate appreciation of the relative accuracies with which the various lateral stability derivatives are extracted can be obtained from the sample vector diagrams (Fig.12). The amplitude ratios between the different degrees of freedom, which determine the length of the vectors, can generally be obtained to about ±5%. The roll/yaw phase angle can be determined to about ±3 degrees and the yaw/sideslip phase angle within about $\frac{1}{2}$ degree. When these conditions hold the derivatives ℓ_p and ℓ_v can be evaluated within about ±10%.

The accuracy with which ℓ_p can be obtained for a specific model from the roll-damping test vehicles depends almost entirely on the magnitude of the rolling moment experienced by the model. At the highest Mach numbers, where the moment is large, the derivative can be determined with an uncertainty of about ±3%, but at transonic and subsonic speeds the uncertainty increases to about ±7%. An additional error may be present in the results from the individual models arising from imperfections in their manufacture such as twist at the wing tips. Careful measurements on each model indicate that this should not exceed 5% of the wing-tip helix angle.

4 THEORETICAL METHODS OF ESTIMATION OF DERIVATIVES

4.1 General background

For the simple configuration chosen (shown in Fig.1), flying at near-zero lift, the theoretical estimation of the derivatives may be based on the linearized theories of potential flow for the wing and fin considered separately, with corrections for the interference effects between the two surfaces being applied to the results. The effects of leading-edge vortex sheets can be ignored. In practice, application of the theories necessitates various approximations being made, which must be proved satisfactory or otherwise for particular types of planform by comparing the results with experimental values. Such comparisons have not previously been made for slender wing designs at transonic and supersonic speeds, for the longitudinal and lateral derivatives.

The wing planform is defined by the relations

$$\left.\begin{aligned} s(x) &= 0.3\,x \quad \text{for} \quad 0 \leq x \leq \tfrac{2}{3} \\ s(x) &= 0.3\,x - 0.45\left(x - \tfrac{2}{3}\right)^2 \quad \text{for} \quad \tfrac{2}{3} < x \leq 1 \end{aligned}\right\} . \qquad (4)$$

with $c_o = 1$.

However, some of the existing computer programmes for various lifting surface theories require that the planform shape be expressed as a polynomial,

$$s(x) = \sum_{1}^{n} a_n x^n , \quad 0 \leq x \leq 1 \qquad (5)$$

and it is found that the "mild gothic" planform given by

$$s(x) = 0.25\,(1.25\,x - 0.25\,x^5) \qquad (6)$$

is very close to the actual planform. The maximum difference in local semispan is 3.3% (at $0.447\,c_o$) and so equation (6) was used when necessary. In addition, an "equivalent" cropped delta planform was chosen, for which charts or algebraic expressions for many of the derivatives have been evaluated. The cropped delta has the same slenderness ratio, $s/c_o = 0.25$, and same parameter $A \tan \Lambda_o$, giving $A = 0.859$ (compared with 0.865), $\Lambda_o = 73.35°$ (73.30°), planform parameter $P = S/bc_o = 0.582$ (0.578) and $\lambda = 0.164$. The conditions at the wing tips must be different for the two planforms, as the discontinuity in leading-edge sweep of the cropped delta implies a discontinuous behaviour of the pressure distribution on the wing along the rearward-going Mach line through the corner, a feature which is not

found with the curved leading edge. However, the resultant total forces and moments may be similar, and, if so, the derivatives of other slender wings could be readily estimated by considering an appropriate cropped delta.

The fin planform is similar to that of the wing but with less leading-edge sweep, and so corresponding equivalent planforms could be chosen.

The thickness distribution of the wing, being diamond spanwise and parabolic chordwise, is amenable to the analysis required for evaluation of thickness corrections. The corresponding correction to the fin contribution is zero, since the section is a flat plate.

4.2 Derivatives due to incidence

(i) Planform contribution

An approximation to supersonic linearized theory has been applied to wing planforms with curved leading edges by Smith in some unpublished work[13], the load distribution being obtained by the cancellation technique in a similar way to that used by Cohen[14] for wings with straight edges. The Mercury programme has been written for planforms given by equation (5), and so the mild gothic, equation (6), has been considered.

An extension to Multhopp's lifting surface theory[15] to supersonic flow has also been programmed[16], mainly with a view to calculating the generalised forces for structural problems. Frequency effects may be evaluated, although for the frequency of the longitudinal short-period oscillation of the free-flight models it should be admissible to assume zero frequency (i.e. steady) conditions. It is again necessary to use equation (6) for the planform.

For the cropped delta planform, charts of lift-curve slope and aerodynamic centre are given in Ref.17, and algebraic expressions have been derived in Refs.18 and 19. There is a restriction on Mach number range, as the theory does not account for interference between the two Mach cones from the wing tips, that is $M \geq 1.2$ for $\lambda = 0.164$ and $s_o/c_o = 0.25$. (The restriction that the leading edge should be subsonic is not significant for the present study, being $M < 3.5$ for sweepback of 73.35°.)

"Not-so-slender" theory may also be used for moderate supersonic speeds, and Squire[20] has obtained the lift-curve slope and aerodynamic centre for the mild gothic planform, defined by equation (6) above, in terms of the parameter $\beta s_o/c_o$. The theory agrees with linearised supersonic theory to order $(\beta s_o/c_o)^2$, so that with $s_o/c_o = 0.25$, and assuming that reasonable accuracy is obtained with $(\beta s_o/c_o)^2 < 0.1$, then the maximum Mach number for which the theory applies is about 1.6.

At M = 1, sonic theory[21] gives $z_w = -\pi A/4$ for the actual planform, and for the equivalent cropped delta, but the positions of the aerodynamic centre on the root chord are different, being dependent on planform shape. At subsonic speeds with the programmes[22] available for Multhopp's lifting surface theory, it is possible to consider the actual planform shape, and to include frequency effects. The cropped delta planform is included in the charts of Ref.23, (Wings S.01.03.03-06 and S.08.01.02), although interpolations have to be made in the region where some of the theoretical curves are themselves fairings between results from Weissinger's compressible lifting line theory[24] and sonic theory. Goodman[25] also gives charts, based on Lawrence's low aspect ratio theory[26], for cropped deltas in incompressible flow, but the method has not been applied to wings with curved leading edges.

(ii) Thickness contributions

Slender body theory, for example Ref.27, indicates a change in pitching moment due to incidence, but no change in overall lift, for thick wings with sharp trailing edges. The conformal transformation required for wings with diamond (spanwise) cross-section has been obtained by Maskell in some unpublished work, and is given in Ref.6. The expression for the rearward shift in aerodynamic centre, as a percentage of root chord, is given as

$$\Delta\bar{x} = \int_0^1 \frac{s^2(x)}{s_o^2}\left[1 - 4\left(\frac{r_o}{s(x)}\right)^2\left(1 - \frac{2\theta}{\pi}\right) + \frac{2}{\pi}\tan\theta\right] dx \qquad (7)$$

where

$$\frac{r_o}{s(x)} = \pi^{\frac{1}{2}}/2\cos\theta\,\Gamma\left(1 - \frac{\theta}{\pi}\right)\Gamma\left(\tfrac{1}{2} + \frac{\theta}{\pi}\right) \qquad (8)$$

and $2\theta(x)$ is the apex angle of the diamond cross-section at the leading edge.

Two-dimensional supersonic theory, extended by strip theory to finite wings, predicts a forward shift of aerodynamic centre due to thickness, (see, for example, the results obtained by Lehrian[28]). For low aspect ratio wings, the results are only valid for large M, but do indicate that there must be an appreciable Mach number effect which cannot be estimated adequately by existing methods. The non-linear thickness correction used by Cooke[29] and others, has not been extended to wings at incidence, as far as is known.

The contributions to z_w from the profile drag has been assumed to be negligible.

(iii) Incidence contribution

Although the models were designed to fly at zero lift, the trim change at sonic speeds gave rise to small trimmed incidences during the subsonic phase of flight, as shown in Fig.6, so that non-linear effects must be considered. The expression for lift suggested in Ref.17, $C_L = \alpha(\pi A/2 + 4|\alpha|)$, based on slender body theory, may be used to give the increment in z_w, and the shift of the aerodynamic centre has been calculated for the mild gothic by Smith in an unpublished extension of the work of Ref.30.

(iv) Fin contributions

The incremental lift and pitching moment induced on the wing due to the fin thickness distribution[31] is independent of incidence, and so contribute nothing to the derivatives.

4.3 Damping-in-pitch derivative, $m_{\dot{\zeta}} = m_q + m_{\dot{w}}$

(i) Planform contribution

The methods of estimation outlined in Ref.32 have been used as far as possible. The lifting surface theories, programmed[16,22] for oscillating wings, are those used for estimating the derivatives due to incidence, and so the same planforms may be considered. For the cropped delta planform, algebraic expressions are given for the derivatives m_q and $m_{\dot{w}}$ at supersonic speeds in Refs.19 and 33 respectively, which although lengthy may be evaluated fairly readily. For subsonic flows, Ref.34 tabulates functions for cropped deltas of effective aspect ratio $A\sqrt{1 - M^2} = 3$, 2 and 1.2, with $\lambda = 1/7$, and these have been extrapolated to zero at $A = 0$ to give the values required for the equivalent cropped delta. Lawrence's[26] theory has also been applied to cropped deltas in incompressible flow, the functions required being given in Refs.25 and 35.

At sonic speeds, although slender body theory gives a value for $m_q + m_{\dot{w}}$ independent of frequency, lifting surface theories[36,37] show a strong dependence, since a term involving $\log \nu_1$ arises. A general formula for low aspect ratio wings is given in Ref.37, and the integrals are more readily evaluated for the actual planform than for the mild gothic.

Not-so-slender theory could be applied directly to obtain m_q, but the load distribution due to acceleration, $\dot{w}$, has not been considered.

(ii) Thickness contribution

Although slender body theory gives m_q and $m_{\dot{w}}$ dependent on the thickness distribution, the oscillatory damping-in-pitch, $m_{\dot{\alpha}} = m_q + m_{\dot{w}}$, is dependent only on the shape at the trailing edge, since the terms due to the thickness distribution are equal but opposite in sign for m_q and $m_{\dot{w}}$. Results for two-dimensional supersonic aerofoils are given in Refs. 28 and 38, but the application of strip theory to obtain finite wing results is only valid at high Mach numbers.

(iii) Incidence contribution

Garner and Lehrian[39] have developed a method for estimating the effects of leading edge separation on the pitching derivatives of a gothic wing, but for the small incidences under consideration the increment is negligible and has not been evaluated.

(iv) Fin contribution

Any interference between the fin and wing in pitch has been neglected.

4.4 Derivatives due to sideslip

4.4.1 Sideforce due to sideslip, y_v

(i) Wing contribution

Although the thickness distribution of the wing will give rise to a sideforce in sideslip, the contribution has been neglected in comparison with that from the fin. Slender body theory[27] gives zero sideforce, being dependent only on the spanwise cross-section shape at the trailing edge.

(ii) Fin contribution

In order to evaluate the lift-curve slope of the fin, the wing is considered to be a complete reflection plate. The planform of the fin with its reflection is similar to that of the wing, but of larger aspect ratio, and so the same methods of estimation could be used as for the incidence derivatives. At supersonic and subsonic speeds the lift-curve slope of the equivalent cropped delta should give sufficient accuracy ($A = 1.37$, $\Lambda_o = 65.5°$, $\lambda = 1/7$), evaluated from Refs.17 and 23 respectively. For low supersonic speeds, $1.0 \leq M \leq 1.2$, not-so-slender theory[20] may be used, and at $M = 1$, $dC_L/d\alpha = \pi A/2$. The sideforce on the fin due to sideslip is then given by

$$y_{v_R} = -\tfrac{1}{2}\frac{S_F}{S}\left(\frac{dC_L}{d\alpha}\right) \qquad (9)$$

where the suffix R denotes the contribution from the fin with its reflection.

(iii) Wing-fin interference

A correction factor to y_{v_R} has been derived[40, 41] from the sideforce of the wing-plus-fin, of the wing alone and of the fin-plus-reflection alone, in the form

$$y_{v_F} = \left[\frac{y_{v_{W+F}} - y_{v_W}}{y_{v_R}} \right] y_{v_R} \qquad (10)$$

the terms inside the square brackets being evaluated by slender body theory. Since the leading edge of the fin remains subsonic for $M < 2.37$, the region of interference is independent of M in the present speed range, and so the interference factor remains constant.

(iv) Incidence contribution

For the small angles of incidence under consideration, the interference effects considered in Refs.40 and 42 may be neglected.

4.4.2 Yawing moment due to sideslip, n_v

(i) Wing contribution

The thickness distribution gives rise to a destabilising (negative) yawing moment, and so, although small, it is necessary to estimate its effect. The integral expression for n_{v_W}, corresponding to equation (7), is given in Ref.6.

(ii) Fin contribution

The position of the aerodynamic centre on the root chord of the fin may be obtained, for the fin-plus-reflection, by the same methods as for the lift-curve slope. The fin section is flat plate, so that no thickness corrections are needed, thus the yawing moment is given by

$$n_{v_R} = -\left(\frac{x_F}{s_o}\right) y_{v_R} \qquad (11)$$

where x_F is the distance of the aerodynamic centre behind the centre of gravity of the model.

(iii) Wing-fin interference

The correction factor to be applied to n_{v_R} is obtained from the analogous relation to equation (10), giving n_{v_F} and so

$$n_v = n_{v_W} + n_{v_F} \quad .$$

(iv) Incidence contribution

The effect of incidence[40, 42] on n_v has been neglected.

4.4.3 Rolling moment due to sideslip, ℓ_v

(i) Wing contribution

The planform and thickness distribution do not contribute directly to the rolling moment, and the wing contribution is considered under (iii) and (iv) below.

(ii) Fin contribution

The height above the wing of the centre of pressure on the fin may be estimated from slender body theory, giving $4s_F/3\pi$, and is independent of Mach number. The rolling moment is then given by

$$\ell_{v_R} = \frac{4}{3\pi}\left(\frac{s_F}{s_o}\right) y_{v_R} \qquad (12)$$

and so is negative.

(iii) Wing-fin interference

There is a large positive rolling moment arising from the pressure induced by the fin on the wing, opposing the fin contribution. At supersonic speeds, the region of interference is confined to the Mach cone from the fin apex, and the pressure distribution on the wing, due to a delta fin, has been evaluated in Ref.43 for Mach numbers such that the Mach lines intersect the trailing edge of the wing, that is $M > 1.75$ for the present configuration. In order to give some idea of the magnitude of the interference effect at lower Mach numbers, the induced pressures were integrated over the wing surface within the Mach cone, neglecting the effect of the wing tip. This should overestimate the magnitude of the induced rolling moment, since the simplification implies that a finite pressure difference exists at the wing leading edge; application of cancellation techniques to correct the difference is not straightforward, as the configuration is non-planar.

At sonic speeds, slender body theory gives the wing-plus-fin rolling moment to be dependent only on the aspect ratio of the wing, and the fin height at the trailing edge, and a simple algebraic expression is given in Ref.44. (It should be noted that the opposite sign to the usual convention for rolling moment has been used.) The interference at subsonic speeds is difficult to determine, but becomes negligible when the angle of incidence is appreciable.

(iv) Incidence contribution

The rolling moment due to combined incidence and sideslip is large and negative for slender wings, and should be estimated even for the small incidences under consideration. The expression derived from supersonic linearised theory[45] is too lengthy to be useful, but slender wing theory should give the accuracy required. Mach number dependence may be approximated by the slender body factor[46] to the loading, as for delta wings. The effect of wing thickness[6] and the presence of the fin[44] may also be obtained separately from slender body theory to give further corrections to the thin wing result.

4.5 Damping-in-roll derivative, ℓ_p

(i) Wing contribution

In principle, any lifting-surface theory may be used for calculating the loading due to steady rolling, the effective downwash being yp at the wing surface. Supersonic linearized theory[18] for the equivalent cropped delta planform leads to an algebraic expression, and at sonic speeds, $\ell_{p_W} = -\pi A/32$. Also, for the cropped delta, Lawrence's low-aspect-ratio theory has been used to obtain charts[35] for subsonic speeds (incompressible flow).

The effect of thickness has been studied for an infinite wing[47] and is found to be small for sections with zero trailing edge thickness.

(ii) Fin contribution

At supersonic speeds, the variation of ℓ_p with Mach number for slender wings is small, and so slender body theory may be used to obtain the loading on the fin. Considering the fin and its reflection, in roll, the effective downwash is $p|z|$, for which the velocity potential must be obtained from the Fourier series[48]

$$\varphi = V_{s_F}(x)\left\{- A_o \sin\theta + \frac{A_1}{4}\sin 2\theta + \sum_2^\infty \frac{A_n}{2}\left[\frac{\sin(n+1)\theta}{n+1} - \frac{\sin(n-1)\theta}{n-1}\right]\right\} \qquad (13)$$

where

$$\frac{w}{V} = \frac{p|z|}{V} = - A_o + \sum_1^\infty A_n \cos n\theta \,, \quad z = s_F(x)\cos\theta$$

and $s_F(x)$ is the local fin height.

The lift on the fin is found to be

$$\frac{C_Y}{\left(\frac{p\, s_F}{V}\right)} = - \frac{2}{3} A_R \quad ,$$

where A_R is the aspect ratio of the fin-plus-reflection and the height of the centre of pressure is given by

$$\frac{\bar{z}}{s_F} = \frac{2}{\pi}\left[\frac{2}{3} + \sum_1^\infty \frac{3}{(4n^2 - 1)(2n + 3)}\left\{\frac{1}{4n^2 - 1} + \frac{1}{4(n+1)^2 - 1}\right\}\right] = \frac{3}{2\pi} \qquad (14)$$

Then

$$\ell_{p_R} = \left(\frac{\bar{z}}{s_F}\right)\frac{C_Y}{\left(\frac{p\, s_F}{V}\right)}\left(\frac{s_F}{s_o}\right)^2 \frac{S_F}{S} \quad . \qquad (15)$$

(iii) Wing-fin interference

The fin interference on the wing is small, but the loading on the wing causes a sidewash on the fin, reducing its effectiveness. For the accuracy required it is sufficient to use the mean value of sidewash evaluated in Ref.6 from slender body theory, so that

$$\ell_{p_F} = \left\{1 - \left[\frac{\partial\sigma}{\partial\left(\frac{pb}{2V}\right)}\right]_{av}\right\}\ell_{p_R} \quad . \qquad (16)$$

(iv) Incidence effects

The effect of incidence on ℓ_p is second order, and may be neglected for the present comparisons.

4.6 Damping-in-yaw derivative $n_r - n_{\dot{v}}$

(i) Wing contribution

The thickness distribution contributes to the steady damping n_r, and slender body theory[27] gives

$$n_{r_W} = -\frac{A}{2}\left(\frac{c_o}{s_o}\right)^2 \int_o^1 (x - x_g)\left(\frac{s}{s_o}\right)^2 \left[\tan\theta - 4\theta\left(\frac{r_o}{s}\right)^2\right] dx \quad , \qquad (17)$$

for the diamond cross-section where r_o/s is given by equation (8). However, the oscillatory damping-in-yaw, $n_r - n_{\dot{v}}$, is zero, being dependent on the thickness at the trailing edge only.

(ii) Fin contribution

As for the sideslip derivatives, the damping-in-yaw due to the fin may be determined from the corresponding longitudinal derivative of the fin with its reflection, that is, n_r from m_q and $n_{\dot{v}}$ from $-m_{\dot{w}}$. The methods of estimation given in Section 4.3 may be used, the lift also having to be evaluated in order to obtain the moment about the centre of gravity position on the wing chord. The conversion to wing representative length and area is given by

$$(n_r - n_{\dot{v}})_R = \left(\frac{\bar{c}_F}{s_o}\right)^2 \frac{S_F}{S}\,(m_q + m_{\dot{w}}) \quad . \qquad (18)$$

An alternative method of estimation, usually used for configurations with the fin mounted on the fuselage some distance behind the wing, is to assume that the incidence distribution $(x - x_g)\,r/V$ due to the steady rate of yaw is equivalent to a constant mean incidence of $x_F\beta$, and that the effect of the acceleration $\dot{\beta}$ is accounted for by a lag in sidewash[49], $-\frac{x_F\dot{\beta}}{V}\frac{d\sigma}{d\beta}$, so that

$$(n_r - n_{\dot{v}})_R = \left(\frac{x_F}{s_o}\right)^2 \left(1 - \frac{d\sigma}{d\beta}\right) y_{v_R} \quad . \qquad (19)$$

However, at zero incidence the only asymmetric loading on the sideslipping wing is that induced by the presence of the fin, so that $d\sigma/d\beta \simeq 0$.

(iii) Wing-fin interference

Slender body theory gives an interference factor equal to that for y_v, since the oscillatory damping-in-yaw is dependent only on the trailing edge configuration.

5 COMPARISON BETWEEN THEORY AND EXPERIMENT

5.1 Lift curve slope, $z_w = -\frac{1}{2} dC_L/d\alpha$, Fig.15

At supersonic speeds the lift curve slope obtained by Smith[13] for the mild gothic planform, gives a satisfactory mean curve for the experimental values for $M > 1.2$. For the application of Multhopp's theory[16] to slender wings, it is necessary to use a relatively large number of lift and downwash points on the wing, and the initial choice of five chordwise and eight spanwise points had to be increased to five chordwise and ten spanwise points (with eleven integration points across the span), before satisfactory agreement with Smith's results for z_w was obtained. The difference in z_w as calculated[16] for steady conditions (zero frequency) and for the experimental frequency is less than $\frac{1}{2}\%$ at $M = 1.4$, and so is negligible. The lift curve slope of the equivalent cropped delta wing[17] is slightly larger than that of the mild gothic planform throughout the supersonic speed range, but the difference is smaller than the experimental scatter. It also appears that not-so-slender theory[20] is applicable only up to about $M = 1.2$, where it gives values close to Smith's linearized theory[13] result, for the present slenderness ratio of $s/c_o = 0.25$, but the experimental value of $-z_w$ at $M = 1.07$ is much greater than the theoretical result.

The theoretical variation of z_w with Mach number subsonically is given for the equivalent cropped delta in steady flow[23], and agrees well with the theoretical value at $M = 0.8$, $\nu = 0.1$, obtained using lifting surface theory[22] for the actual planform. The experimental value of $-z_w$ at $M = 0.93$ was obtained from a model flying at $C_{L_{Trim}} \simeq -0.03$, and so the non-linear contribution to z_w has been evaluated, the increment being shown in Fig.15 for $0.8 < M < 1.0$. The agreement between experiment and theory is excellent, although this may be fortuitous, as there is appreciable scatter between the experimental values at supersonic speeds.

5.2 Manoeuvre margin, $h - h_o$, Fig.16

The theoretical position of the aerodynamic centre appears to be further forward than that obtained experimentally over most of the Mach number range, and there is about 4% $\bar{c}$ overall difference between the results of the theories of Refs.13, 16 and 17. At M = 1.4, the theoretical results from Ref.16 for zero frequency and finite (experimental) frequency agree, and so Smith's steady theory[13] is the most rigorous method of estimation. It appears that even more Multhopp points on the wing would have to be considered before agreement is achieved between the results of Refs.16 and 13, although increasing the number of spanwise downwash points from eight to ten and integration points from eight to eleven reduced the difference from 5.5% $\bar{c}$ to 1.5% $\bar{c}$ at M = 1.4 and from 16.6% $\bar{c}$ to 2.0% $\bar{c}$ at M = 2.0.

The theoretical results for the equivalent cropped delta are about 2% $\bar{c}$ rearward of the results of Ref.13, but at subsonic speeds agree with the subsonic lifting surface theory[22] at M = 0.8. Thus the theoretical variation of aerodynamic centre position with Mach number is best assessed from the Data Sheets[23] (plus the non-linear contribution) for $M < 1.0$, not-so-slender theory for $1.0 < M < 1.2$, and Smith's theory for $M > 1.2$, so that up to about M = 1.5, the average difference between experiment and theory is 4% $\bar{c}$. For $M > 1.6$, although the experimental results and theoretical curves are in closer agreement, the variation with M appears to be different, with the experimental aerodynamic centre moving forward as M increases, and the theoretical position continuing to move rearward, up to M = 2.1, before beginning to move forward. As mentioned in Section 4.2, this discrepancy may be due to the effect of thickness. A constant increment, $\Delta h = 0.033$ from equation (7), has been added to the thin wing results, although it is known that Δh becomes negative at higher Mach numbers, according to strip and piston theories. Van Dyke's thick aerofoil results have also been evaluated, and used with strip theory, but this gives $\Delta h = -0.05$ and -0.035 at M = 1.8 and 2.2 respectively that is, again in the opposite sense to experiment; these latter increments have not been included in the theoretical results shown in Fig.16.

5.3 Pitching moment due to incidence, m_w, Fig.17

Since $m_w = (h - h_o)\, z_w$, the difference between estimated and experimental position of the aerodynamic centre is also apparent in the results for the pitching moment. The experimental trend is more clearly defined for m_w, (since this can be obtained directly from the frequency of the longitudinal oscillation

and requires only small corrections for change of c.g. position for the various models) and there is little scatter between the results. A striking difference between experiment and theory occurs in the transonic region, for which no explanation can be given. At subsonic speeds, the same trend with Mach number is given by experiment and theory[23], but the experimental results for $-m_w$ are about 0.025 greater than the theoretical curve, even when the increment, $\Delta m_w = -0.015$, due to non-linear incidence effects is included. At M = 1.0, the measured m_w is 50% greater in magnitude than estimated, but experiment and theory converge as M increases supersonically until agreement is reached at about M = 1.7.

A constant increment of $\Delta m_w = -0.022$ due to thickness has been included throughout the speed range, and corresponding remarks to those in Section 5.2 about the possible variation of thickness effects with Mach number also apply to the estimation of m_w.

5.4 Damping-in-pitch derivative $m_{\dot\eta} = m_q + m_{\dot w}$, Fig.18

Supersonic linearised theory[19,33] for the cropped delta planform and lifting surface theory for the mild gothic planform[16] overestimate the damping, the error increasing as M increases. Part of this may be due to thickness effects, which can be significant, but again the only method of estimation is to use strip theory with the aerofoil theories of either Ref.28 or 38. An increase in damping is indicated at M = 1.4 ($\Delta m'_{\dot\eta} \simeq -0.02$), with a slight decrease at M = 1.8 and 2.2 ($\Delta m'_{\dot\eta} = 0.005$ and 0.007 respectively), but these increments have not been included in the theoretical curve in Fig.18 as the application of strip theory to slender wings does not seem justified.

The theory of Ref.16 is essentially oscillatory for the estimation of the damping, and so no comparison can be made with steady results at supersonic speeds. At M = 1.0, where frequency effects are important, slender body theory[27] gives $m'_{\dot\eta} = -0.51$, independent of frequency, whereas oscillatory theory[37] at sonic speeds gives $m'_{\dot\eta} = -0.54$ for $\omega\bar{c}/V = 0.11$, the experimental frequency. It is difficult to establish absolutely the trend of the experimental results in the sonic region, but all the theoretical estimates appear to be too large in magnitude. Although the interpolations made on the results given in Ref.34 do indicate lower values of damping subsonically, the value at M = 0.8 does not agree with the lifting surface calculation, Ref.22.

5.5 Sideforce due to sideslip y_v, Fig.19

The theoretical estimate of y_v agrees very well with the experimental results throughout the supersonic speed range. The lift curve slope of the cropped delta "equivalent" to the fin planform has been used for the supersonic and subsonic regions (Refs.17 and 23), and that of the mild gothic (Ref.20) at low supersonic speeds. y_v is possibly overestimated slightly for $1.0 < M < 1.2$, and for $M >$ about 1.7, but the error is not significant.

5.6 Yawing moment due to sideslip, n_v, Fig.20

The same theories have been used for estimating n_v as for y_v, and the results agree quite well with experiment, indicating the transonic increase in n_v, and the decrease (i.e. loss of directional stability), as M increases further. At supersonic speeds, the experimental results exhibit differences due to the different fin shapes under test. One of the early models (5) had an actual cropped delta fin, and the results obtained are shown by the triangular symbols. These are seen to be above the results from models with the fin with rounded tip, and the loss of n_v as M increases is greater. The corresponding theoretical estimates are shown by the dashed and full curves respectively, and the difference caused by the change of fin shape is seen to be opposite to that found experimentally. This suggests that a different choice of "equivalent" cropped delta for the fin with rounded tip might give closer correlation between experiment and theory, as the variation with Mach number agrees well, there being a constant difference of 0.017 between theory and the experimental mean curve. However, no attempt has been made to adjust the theoretical estimate on this basis. The difference in the variation with M for the results of model 5 is probably due to tip loss effects on the actual cropped delta, which cannot be accounted for theoretically, and which are eliminated experimentally by rounding the tips.

The experimental results at transonic speeds are greater than the theoretical curve, implying that the centre of pressure on the fin is further aft than calculated. A similar difference was noted in the comparison of experimental and theoretical results for m_w and static margin (paras. 5.2 and 5.3).

5.7 Rolling moment due to sideslip, ℓ_v, Fig.21

Theoretically, the two major contributions to ℓ_v are of opposite sign[43], and comparable magnitude, and the estimates are plotted separately in Fig.21(b) and combined in Fig.21(a) for comparison with experiment. The fin contribution

is negative, while the induced pressures on the wing give rise to a positive rolling moment, both contributions decreasing in magnitude as M increases. (The dashed part of the curve is that obtained by neglecting wing tip effects on the induced pressures (see Section 4.4.3), and is an overestimate of the wing-fin interference effect.) The resultant estimate of ℓ_v gives the correct variation with M, but there is an almost constant difference of about 0.008 between experiment and theory. However, an error of this magnitude is not significant when considered relative to the magnitudes of the separate contributions. Slender body theory[44] gives $\ell_v = +0.0083$ at M = 1, which is in reasonable agreement with the experimental results.

For the test flight which established the experimental variation of ℓ_v between M = 1.2 and 1.6, the model flew at a small negative trimmed C_L at the lower supersonic Mach numbers (e.g. $C_L = -0.004$ at M = 1.2 and $C_L = -0.002$ at M = 1.4), and so the increment in ℓ_v due to incidence is also indicated on Fig.21. The estimated increment for the test flight under consideration is shown in Fig.21(b), and the constant increment for $C_L = -0.004$ is shown in Fig.21(a).

5.8 Damping-in-roll derivative, ℓ_p Fig.22

The theoretical estimate[18] of the damping in roll of the equivalent cropped delta planform is about 10% greater than that obtained experimentally from the steady rolling tests at supersonic speeds, showing little variation with Mach number between M = 1.2 and 2.3 (see Fig.22(a)). The experimental results obtained from the oscillatory tests possibly indicate a reduction in damping as M increases above about 1.6, but the trend is not sufficiently established to warrant any revision of the theoretical estimate*. No explanation can be given of the experimental reduced damping at low supersonic speeds (M = 1.07 and 1.15). At M = 1.0, sonic theory[21] and the experimental results from the steady rolling tests agree well, but subsonically the estimate based on incompressible flow theory[35] is below the experimental curve.

The theoretical fin contribution to the damping is $\ell_{p_F} = -0.0044$, independent of M, which agrees well with the experimental results shown in Fig.22(c) for

* Values were obtained from lifting surface theory[16] at M = 1.4 and 2.0, which did show a reduction in damping at the higher Mach number, but it was not possible with the present Mercury programmes to increase the number of spanwise points in the calculations sufficiently to confirm the results.

wing alone and wing with two fins, above and below the wing, where the experimental increment must be compared with 2 ℓ_{p_F}.

5.9 Damping-in-yaw derivative $n_r - n_{\dot{v}}$, Fig.23

The estimate based on the oscillatory damping of the fin[19,33] gives greater damping than the approximate values obtained from the sideslip derivatives, and is in better agreement with the experimental results at the low supersonic speeds. At the higher supersonic speeds, the two estimates converge, and are close to the experimental values. At sonic speeds, the result from slender body theory[27] is in agreement with the experimental trend, which indicates increased damping in the sonic region. The theoretical subsonic results[34] are shown for completeness although there are no experimental results for comparison.

6 CONCLUSIONS

Free-flight experiments have yielded values of the longitudinal and lateral stability derivatives for a slender wing-plus-fin design. The results were obtained at near-zero lift conditions throughout the speed range, M = 0.8 to 2.4, and are compared with the theoretical estimates.

The experimental values obtained from the various models are consistent, with little scatter in the results for the derivatives due to incidence and sideslip. The damping derivatives are more difficult to analyse from the experimental data, so that greater scatter is evident, but the variation of the derivatives with Mach number is clearly defined. The damping-in-roll has also been obtained from steady rolling models, and the results agree well with those obtained from analysis of the Dutch-roll oscillation and the roll subsidence damping, except in the transonic region.

The theoretical results are based on existing methods of estimation. In principle, it is possible to calculate the major contributions to all the derivatives using lifting-surface theories, some of which have been programmed for digital computers, and theoretical results are given for some specific Mach numbers and frequencies. However, these programmes are lengthy, so two further sets of theoretical results have been evaluated in order to check the validity of the more simple theories. First, for supersonic speeds, not-so-slender theory and the lift-cancellation technique have been applied, for small incidences, to a "mild gothic" planform, which is very close to the actual planform of the models, so that the range M = 1.0 to 2.0 has been covered for the derivatives due to incidence and sideslip. Second, an "equivalent" cropped delta planform has been chosen for which algebraic expressions or charts exist for most of the derivatives throughout the speed range. Where comparison

between the various theoretical results is possible, the agreement is good, and the difference is usually less than the experimental scatter.

The agreement between experimental and theoretical results is reasonable, although the difference in manoeuvre margin at transonic speeds is appreciable, even when the non-linear contribution due to the trimmed angle of incidence is included. The experimental values of all the moment derivatives (except ℓ_v) also indicate greater dependence on Mach number, for M greater than about 1.6, than is given by the theoretical results, but this may be due to the failure of existing theories to account for thickness effects at such speeds. However, the overall agreement is sufficiently good to enable one to estimate derivatives for similar slender wing designs with a fair degree of confidence, by applying correction factors, obtained from the present comparison, to the theoretical results.

It should perhaps be reiterated here that the model design tested was purposely chosen to be a simple wing-plus-fin, so that the basic theories could be checked. Further tests will enable comparisons to be made for a lifting wing, when non-linear incidence effects may become important, and larger interference effects of the wing on the fin could be expected. These effects are more difficult to estimate theoretically, but are essentially added contributions and corrections to the linear theories considered here.

Table 1

Model data

Geometry

Wing:	Planform area	12.813 ft^2
	Aspect ratio	0.865
	Planform parameter, P	0.578
	Span/length ratio	0.5
	Geometric mean chord, $\bar{c}$	3.853 ft
	Volume	1.926 ft^3
	Thickness/chord ratio on centre line	0.065
	Newby area distribution	4st x (1-x)
	Zero camber and twist	
Fin:	Area (gross)	1.281 ft^2
	Aspect ratio	0.695
	Geometric mean chord, $\bar{c}_F$	1.379 ft
Centre of gravity		0.50 c_o

Typical weight and inertias

Weight	208 lb
Inertia in roll, I_x	1.40 slug ft^2
Inertia in pitch, I_y	16.78 slug ft^2
Inertia in yaw, I_z	16.96 slug ft^2
Product of inertia, I_{xz}	0.136 slug ft^2

SYMBOLS

A	aspect ratio
A_n, a_n	coefficients in series (equations (13) and (5))
a_y	lateral acceleration at the centre of gravity, ft/s^2
b	span
C_L	lift coefficient, $L/\frac{1}{2}\rho V^2 S$
c_o	root chord
$\bar{c}$	geometric mean chord
$\bar{c}_F$	geometric mean chord of fin
e_x	$= - I_{xz}/I_x$
e_z	$= - I_{xz}/I_z$
g	acceleration due to gravity, ft/s^2
h	position of aerodynamic centre on $\bar{c}$
h_o	position of centre of gravity on $\bar{c}$
I_x, I_y, I_z	moments of intertia in roll, pitch and yaw, respectively slug ft^2
I_{xz}	product of inertia, slug ft^2
i_x	$= I_x/ms_o^2$
i_z	$= I_z/ms_o^2$
k	damping index of roll subsidence mode
L	lift
$\mathscr{L}$	rolling moment
L_p, L_r, L_v	rolling moment derivatives, e.g. $L_p = \partial\mathscr{L}/\partial p$
ℓ_p	$= L_p/\frac{1}{4}\rho V S b^2$
ℓ_r	$= L_r/\frac{1}{4}\rho V S b^2$
ℓ_v	$= L_v/\frac{1}{2}\rho V S b$
M	Mach number
$\mathscr{M}$	pitching moment
M_q, M_w, $M_{\dot{w}}$	pitching moment derivatives, e.g. $M_q = \partial\mathscr{M}/\partial q$
m	mass of model
m_q	$= M_q/\rho S V \bar{c}^2$
m_w	$= M_w/\rho S V \bar{c}$
$m_{\dot{w}}$	$= M_{\dot{w}}/\rho S \bar{c}^2$
m_ϑ	$= m_q + m_{\dot{w}}$
$\mathscr{N}$	yawing moment
N_p, N_r, N_v, $N_{\dot{v}}$	yawing moment derivatives, e.g. $N_p = \partial\mathscr{N}/\partial p$

SYMBOLS (Contd)

n_p	$= N_p/\frac{1}{4}\rho V S b^2$
n_r	$= N_r/\frac{1}{4}\rho V S b^2$
n_v	$= N_v/\frac{1}{2}\rho V S b$
n'_v	$= N_v/\frac{1}{4}\rho S b^2$
P	planform parameter, S/bc_o
p	rate of roll, rad/s
q	rate of pitch, rad/s
R_e	Reynolds number
R	ratio of amplitude in Dutch-roll mode $\left(\text{e.g. } R_{a_y\beta} = \frac{\text{amplitude in } a_y}{\text{amplitude in } \beta}\right)$
r	rate of yaw, rad/s
r_o	defined in equation (8)
S	wing area
S_F	fin area
s_o	wing semispan at trailing edge
s_F	height of fin
s(x)	local semispan of wing } based on $c_o = 1$
$s_F(x)$	local height of fin } based on $c_o = 1$
$\hat{t}$	unit of aerodynamic time, $m/\rho S V$
V	velocity along flight path
v	lateral perturbation velocity
w	normal perturbation velocity
x	chordwise coordinate, with $c_o = 1$
x_F	distance between centre of gravity and centre of pressure of fin
x_g	distance of centre of gravity aft of wing apex, with $c_o = 1$
Y	sideforce
Y_v	sideforce derviative due to sideslip, $Y_v = \partial Y/\partial v$
y_v	$= Y_v/\rho S V$
y	lateral coordinate
Z	normal force
Z_w	normal force derivative due to normal velocity, $Z_w = \partial Z/\partial w$
z_w	$= Z_w/\rho S V$
z	normal coordinate
$\bar{z}$	height of centre of pressure of fin

SYMBOLS (Contd)

α	angle of incidence, rad ($\simeq w/V$)
β	angle of sideslip, rad ($\simeq v/V$) $\sqrt{M^2 - 1}$ in section 4.2
Γ	gamma function
θ	spanwise parameter, equation (13)
$\theta(x)$	local apex angle of diamond cross-section at the leading edge
Λ_o	sweepback angle of leading edge
λ	taper ratio
λ_1, λ_2	total damping of longitudinal short-period and Dutch-roll oscillations respectively
μ_2	relative density parameter, $m/\rho\ Ss_o$
ν_1	frequency of longitudinal short-period oscillation, rad/s
ν_2	frequency of lateral (Dutch-roll) oscillation, rad/s
ν_{c_1}	$= \nu_1/2\pi$, c/s
ν_{c_2}	$= \nu_2/2\pi$, c/s
ρ	air density, slug/ft^3
σ	sidewash angle, rad
ϕ	phase angle (e.g. ϕ_{rp} is phase advance of r relative to p)
φ	velocity potential
ω_2	undamped natural frequency of lateral oscillation, rad/s

Suffixes

F	fin
R	reflected fin
W	wing contribution
W + F	wing-plus-fin contribution

REFERENCES

No.	Author	Title, etc.
1	A. Doyle	Unpublished Mintech Report
2	A. J. Ross	The lateral oscillation of slender aircraft. R.A.E. Report Aero 2666, A.R.C. C.P. 845, June 1962
3	W. J. G. Pinsker	The lateral motion of aircraft, and in particular of inertially slender configurations. A.R.C. R. & M. 3334, September 1961
4	P. L. Bisgood	Low-speed investigations using free-flight models. R.A.E. Tech. Note Aero 2713, A.R.C. 22459, 1960
5	H. H. B. M. Thomas	Estimation of stability derivatives (State of the Art). A.R.C. C.P. 664, August 1961
6	A. J. Ross	The calculation of lateral stability derivatives of slender wings at incidence, including fin effectiveness, and correlation with experiment. A.R.C. R. & M. 3402, March 1961
7	J. S. Thompson R. A. Fail	Oscillatory derivative measurements on sting-mounted wind tunnel models. Method of test and results for pitch and yaw on a cambered ogee wing at Mach numbers up to 2.6. A.R.C. R. & M. 3355, July 1962
8	K. J. Turner	The measurement of aileron rolling power and roll damping by free-flight models at Mach numbers up to 2.5. A.R.C. C.P. 679, March 1958
9	J. A. Hamilton P. A. Hufton	Free-flight techniques for high-speed aerodynamic research. Jour.Roy.Aero.Soc., March 1956

REFERENCES (Contd)

No.	Author	Title, etc.
10	K. H. Doetsch	The time-vector method for stability investigations. A.R.C. R. & M. 2945, August 1953
11	K. J. Turner	Measurements of dynamic stability from three simplified free-flight models of a supersonic research aircraft (Bristol T.188) over the Mach number range 1.2 - 2.6. A.R.C. C.P. 816, March 1961
12	J. Picken	The uncertainty of processed data from free-flight experiments. R.A.E. Tech. Note Aero 2604, February 1959
13	J. H. B. Smith	R.A.E. Unpublished work.
14	D. Cohen	The theoretical lift of flat swept-back wings at supersonic speeds. NACA Tech. Note 1555, March 1948
15	H. Multhopp	Methods for calculating the lift distribution of wings. (Subsonic lifting surface theory) A.R.C. R. & M. 2884, January 1950
16	G. Z. Harris	Mercury programmes for lifting surface theory calculations on wings oscillating in supersonic flow. A.R.C. C.P. 851, November 1964
17	J. H. B. Smith J. A. Beasley A. Stevens	Calculations of the lift slope and aerodynamic centre of cropped delta wings at supersonic speeds. A.R.C. C.P. 562, July 1960
18	F. S. Malvestuto K. Margolis H. S. Ribner	Theoretical lift and damping-in-roll at supersonic speeds of thin sweptback tapered wings with streamwise tips, subsonic leading edges and supersonic trailing edges. NACA Report 970, 1950

REFERENCES (Contd)

No.	Author	Title, etc.
19	F. S. Malvestuto D. M. Hoover	Lift and pitching derivatives of thin sweptback tapered wings with streamwise tips and subsonic leading edges at supersonic speeds. NACA Tech. Note 2294, 1951
20	L. C. Squire	Some applications of "not-so-slender" wing theory to wings with curved leading edges. A.R.C. R. & M. 3278, July 1960
21	K. W. Mangler	Calculation of the pressure distribution over a wing at sonic speeds. A.R.C. R. & M. 2888, September 1951
22	D. E. Davies	Calculation of unsteady generalised airforces on a thin wing oscillating harmonically in subsonic flow. A.R.C. R. & M. 3409, August 1963
23		Data sheets. Aerodynamics. Roy.Aero.Soc.
24	J. DeYoung C. W. Harper	Theoretical symmetric span loading at subsonic speeds for wings having arbitrary planform. NACA Report 921, 1948
25	A. Goodman	Calculation of aerodynamic characteristics of low-aspect-ratio wings at subsonic speeds. Cornell Aero Lab. Report AF-743-A-1, 1951
26	H. R. Lawrence	The lift distribution on low-aspect-ratio wings at subsonic speeds. Journ. Aero. Sci. Vol.18, No.10, October 1951
27	A. H. Sacks	Aerodynamic forces, moments and stability derivatives for slender bodies of general cross-section. NACA Tech. Note 3283, 1954
28	D. E. Lehrian	Calculation of stability derivatives for tapered wings of hexagonal planform oscillating in a supersonic stream. A.R.C. R. & M. 3298, September 1960

REFERENCES (Contd)

No.	Author	Title, etc.
29	J. C. Cooke	Slender not-so-thin wing theory. A.R.C. C.P. 659, January 1962
30	J. H. B. Smith	A theory of the separated flow from the curved leading edge of a slender wing. A.R.C. R. & M. 3116, November 1957
31	L. B. Jones	The effects on wing lift and pitching moment due to the fin of an aircraft flying at supersonic speeds. English Electric Aero Research. Report 1, 1961
32	H. H. B. M. Thomas B. F. R. Spencer	The calculations of the derivatives involved in the damping of the longitudinal short-period oscillations of an aircraft and correlation with experiment. R.A.E. Report Aero 2561, A.R.C. 18498, November 1955
33	F. S. Malvestuto D. M. Hoover	Supersonic lift and pitching moment of thin swept-back tapered wings produced by constant vertical acceleration. Subsonic leading edges and supersonic trailing edges. NACA Tech. Note 2315, 1951
34	H. C. Garner	Multhopp's subsonic lifting-surface theory of wings in slow pitching oscillations. A.R.C. R. & M. 2885, July 1952
35	H. N. Stone	Aileron characteristics and certain stability derivatives for low-aspect-ratio wings at subsonic speeds. Cornell Aero Lab. Report AF-743-A-3, 1952
36	K. W. Mangler	A method of calculating the short-period longitudinal stability derivatives of a wing in linearised unsteady compressible flow. A.R.C. R. & M. 2924, June 1952

REFERENCES (Contd)

No.	Author	Title, etc.
37	M. I. Landahl	The flow around oscillating low-aspect-ratio wings at transonic speeds. K.T.H. Aero. Tech. Note 40, 1954
38	J. C. Martin N. Gerber	The effect of thickness on aerofoils with constant vertical acceleration at supersonic speeds. J.Aero.Sci. Vol.22, No.3, 1955
39	H. C. Garner D. E. Lehrian	Pitching derivatives for a gothic wing oscillating about a mean incidence. A.R.C. C.P. 655, February 1963
40	J. N. Neilsen G. E. Kaattari	The effect of vortex and shock expansion fields on pitch and yaw instabilities of supersonic airplanes. I.A.S. Preprint, 743, 1957
41	F. K. Goodwin G. E. Kaattari	Estimation of directional stability derivatives at small angles and subsonic and supersonic speeds. NASA TIL 6338, 1958
42	G. E. Kaattari	Estimation of directional stability derivatives at moderate angles and supersonic speeds. NASA TIL 6349, 1959
43	F. S. Malvestuto	Theoretical supersonic force and moment coefficients on a sideslipping vertical and horizontal tail combination with subsonic leading edges and supersonic trailing edges. NACA Tech. Note 3071, 1954
44	C. C. L. Sells	Calculation of sideslip derivatives and pressure distribution in asymmetric flight conditions on a slender wing-fin configuration. R.A.E. Tech. Note Aero 2805, A.R.C. 23788, January 1962
45	K. Margolis W. L. Sherman M. E. Hannah	Theoretical calculation of the pressure distribution, span loading and rolling moment due to sideslip at supersonic speeds for thin sweptback tapered wings with supersonic trailing edges and wing tips parallel to the axis of wing symmetry. NACA Tech. Note 2898, 1953

REFERENCES (Contd)

No.	Author	Title, etc.
46	H. S. Ribner F. S. Malvestuto	Stability derivatives of triangular wings at supersonic speeds. NACA Tech. Note 1572, 1948
47	J. C. Martin M. Gerber	On the effect of thickness on the damping in roll of airfoils at supersonic speeds. Ball. Res. Lab. Report 843, 1953
48	H. S. Ribner	The stability derivatives of low-aspect-ratio triangular wings at subsonic and supersonic speeds. NACA Tech. Note 1423, 1947
49	L. R. Fisher H. S. Fletcher	Effect of lag of sidewash on the vertical-tail contribution to oscillatory damping in yaw of airplane models. NACA Tech. Note 3356, 1955

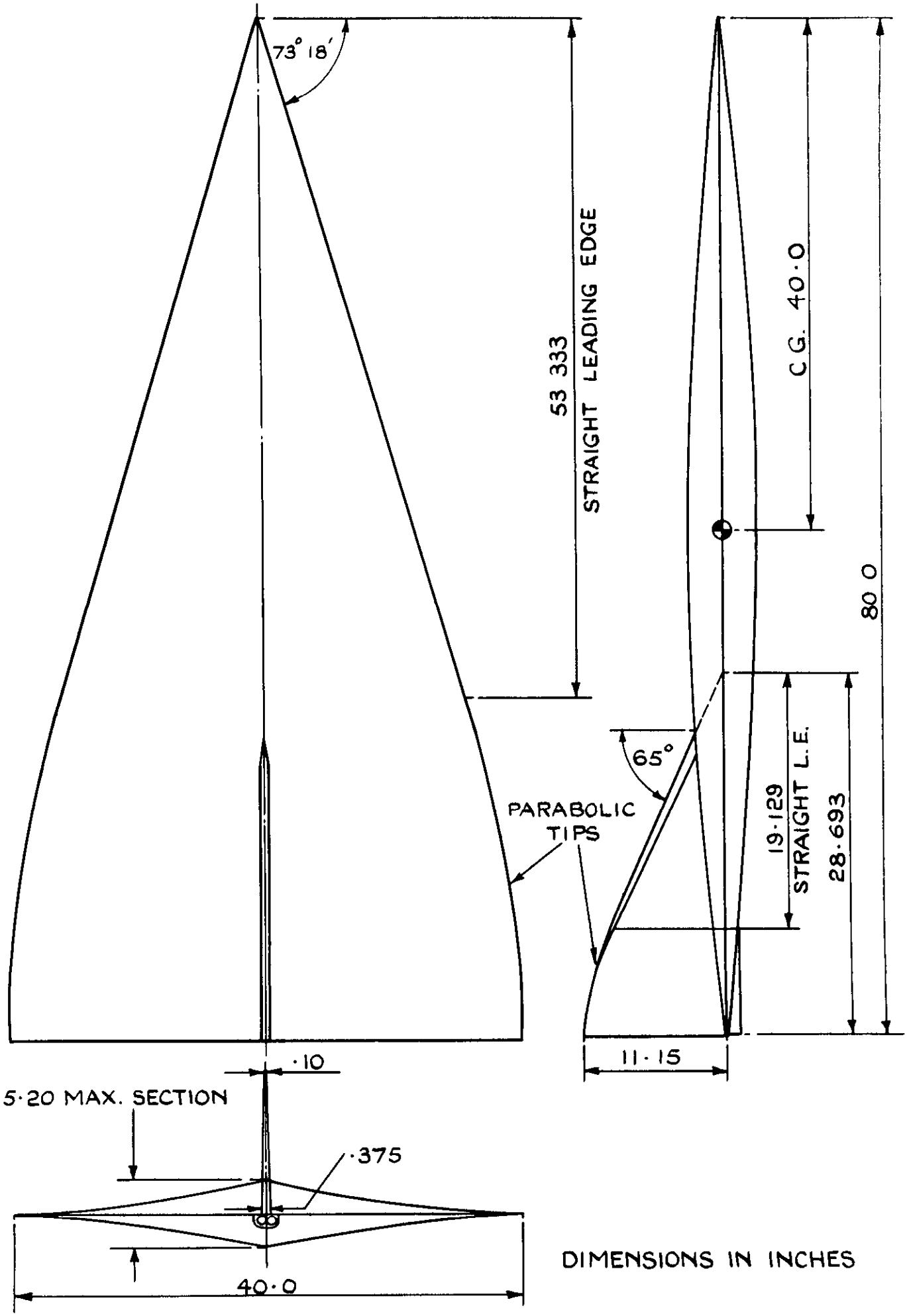

FIG. 1 MODEL GEOMETRY

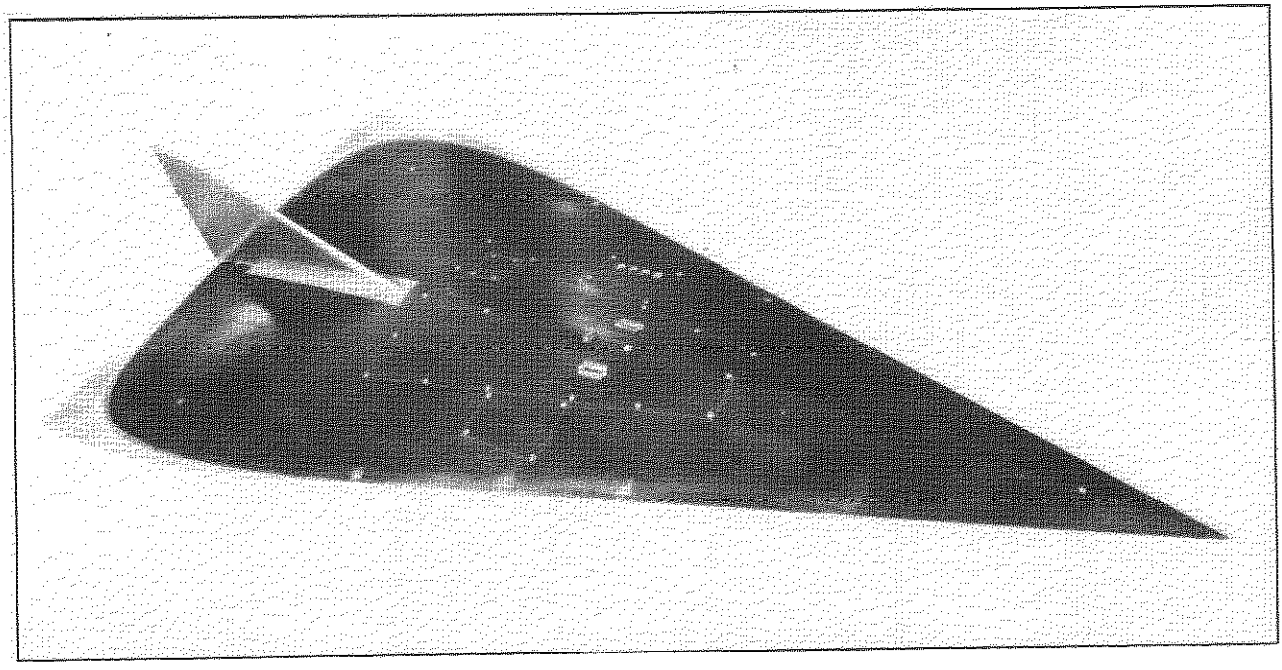

Fig.2a. Complete model

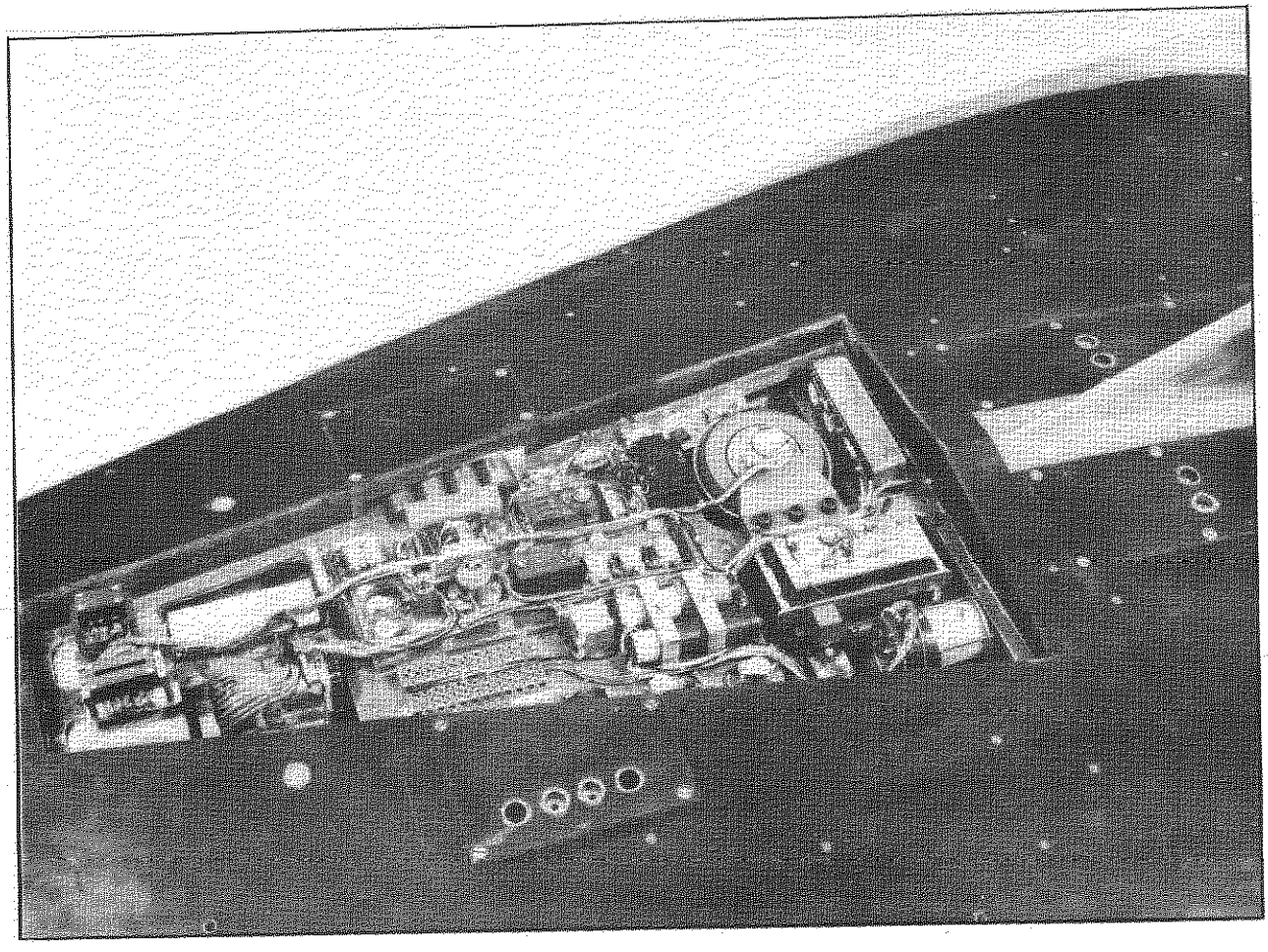

Fig.2b. Instrumentation bay

Fig.2 Models

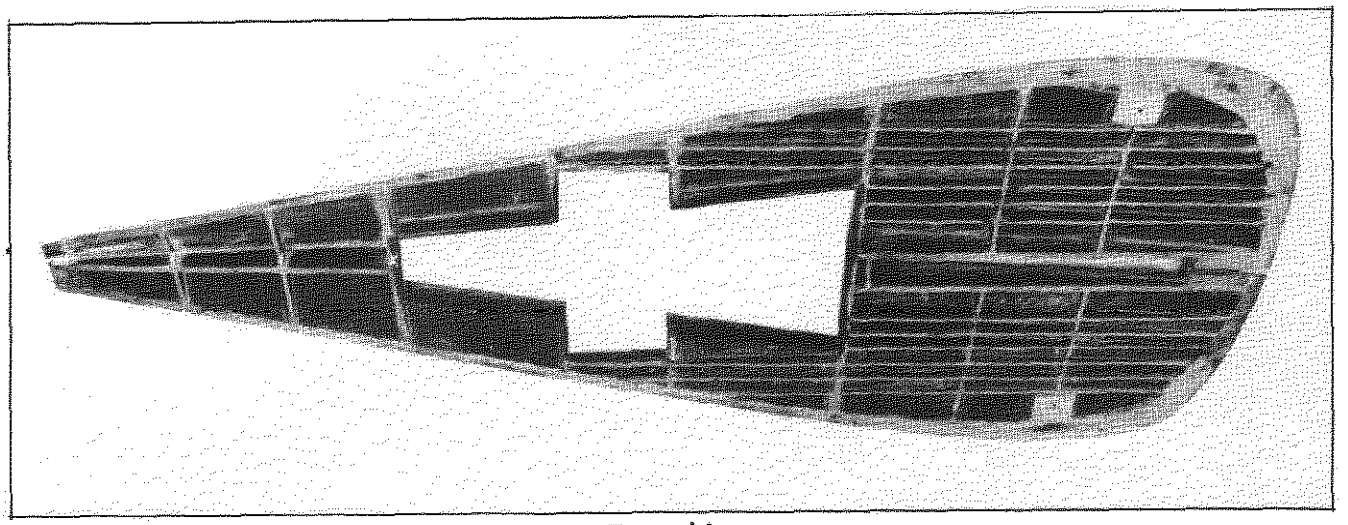

Top skin

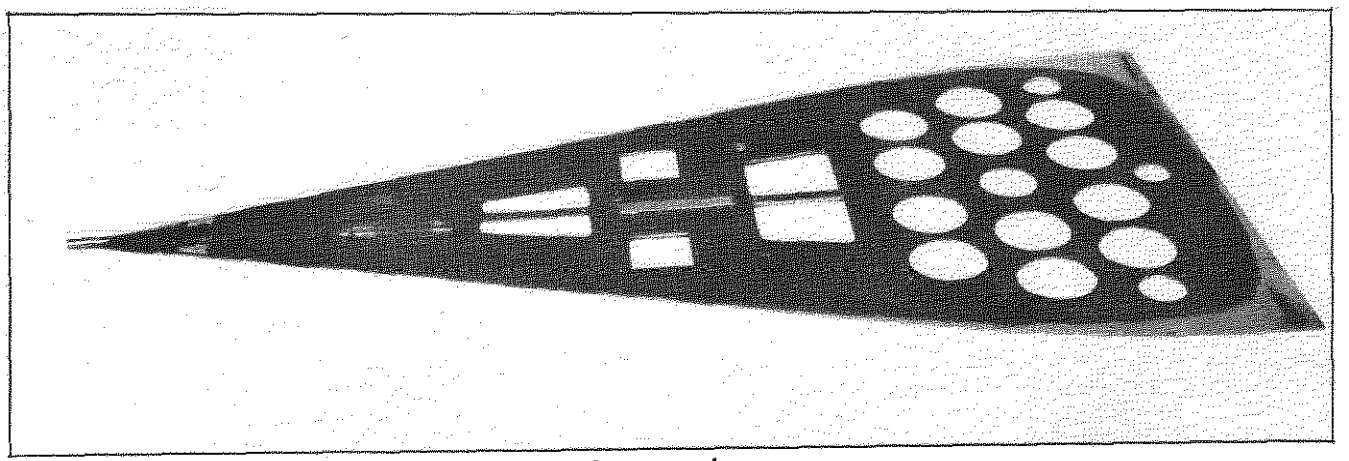

Centre plate

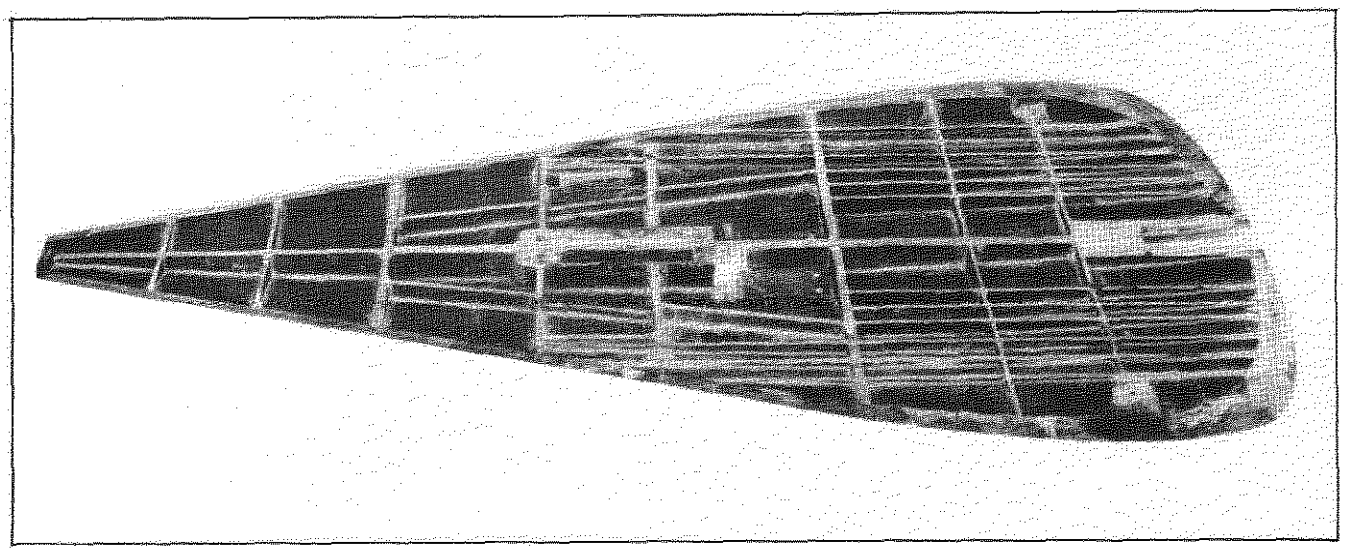

Bottom skin

Fig.2c. Model structure

Fig.2Cont'd. Models

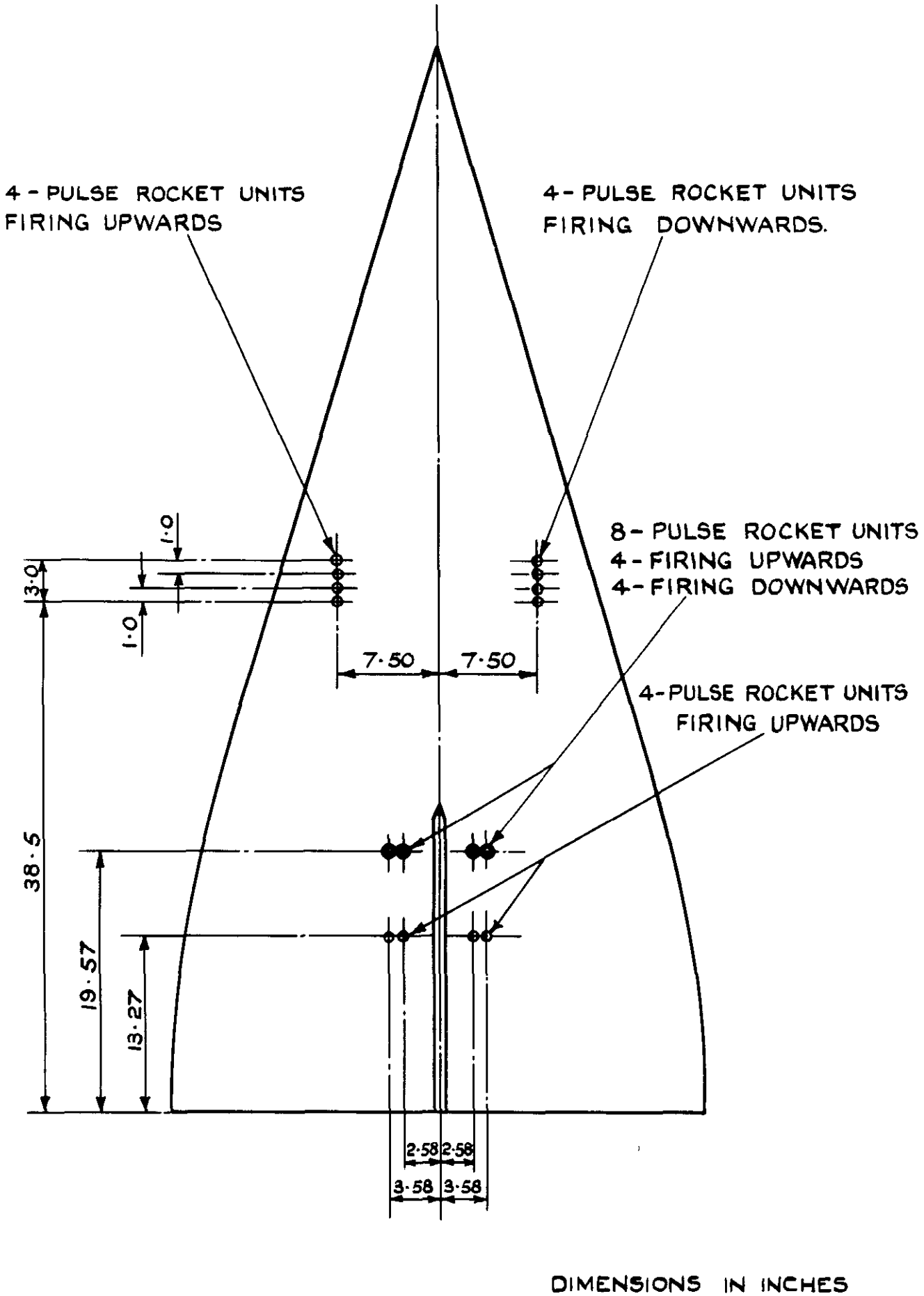

FIG. 3(a) TYPICAL PULSE-ROCKET ARRANGEMENT

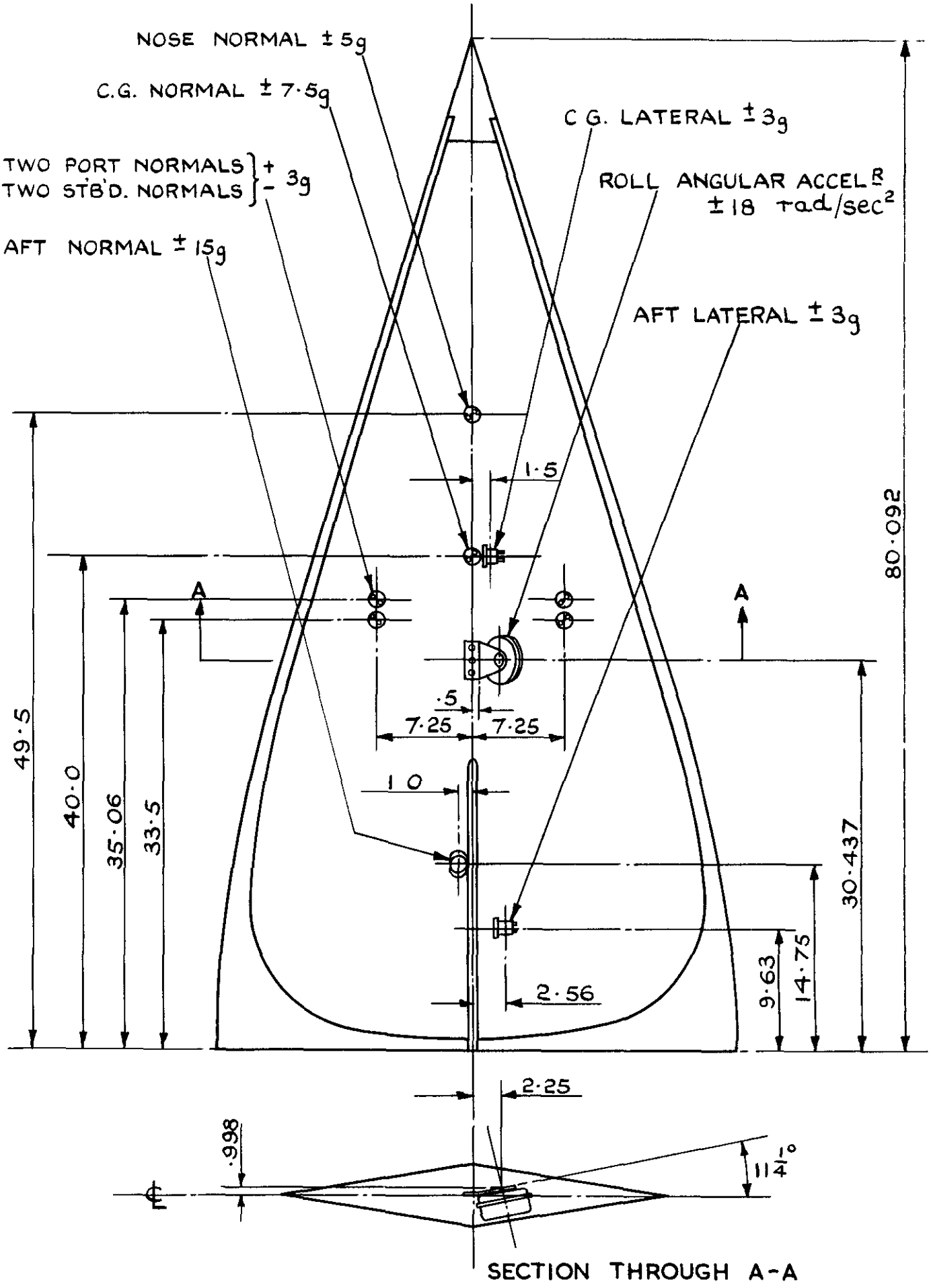

FIG. 3(b) TYPICAL ACCELEROMETER ARRANGEMENT

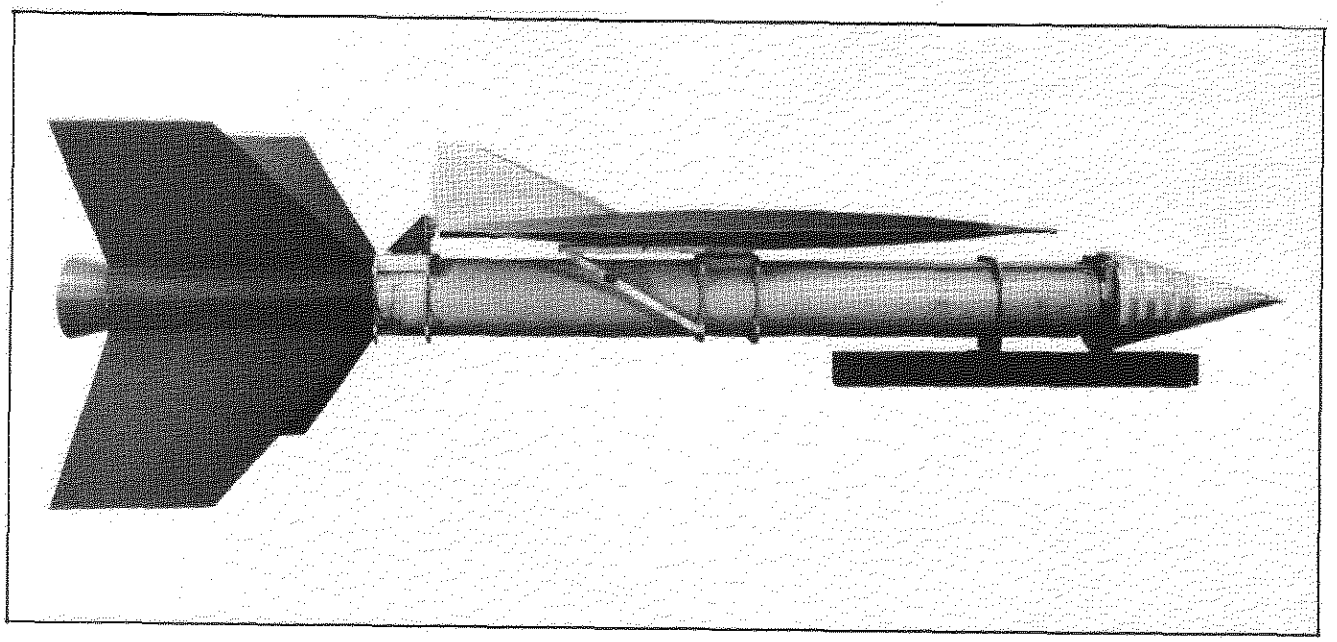

Fig.4a. Boost assembly

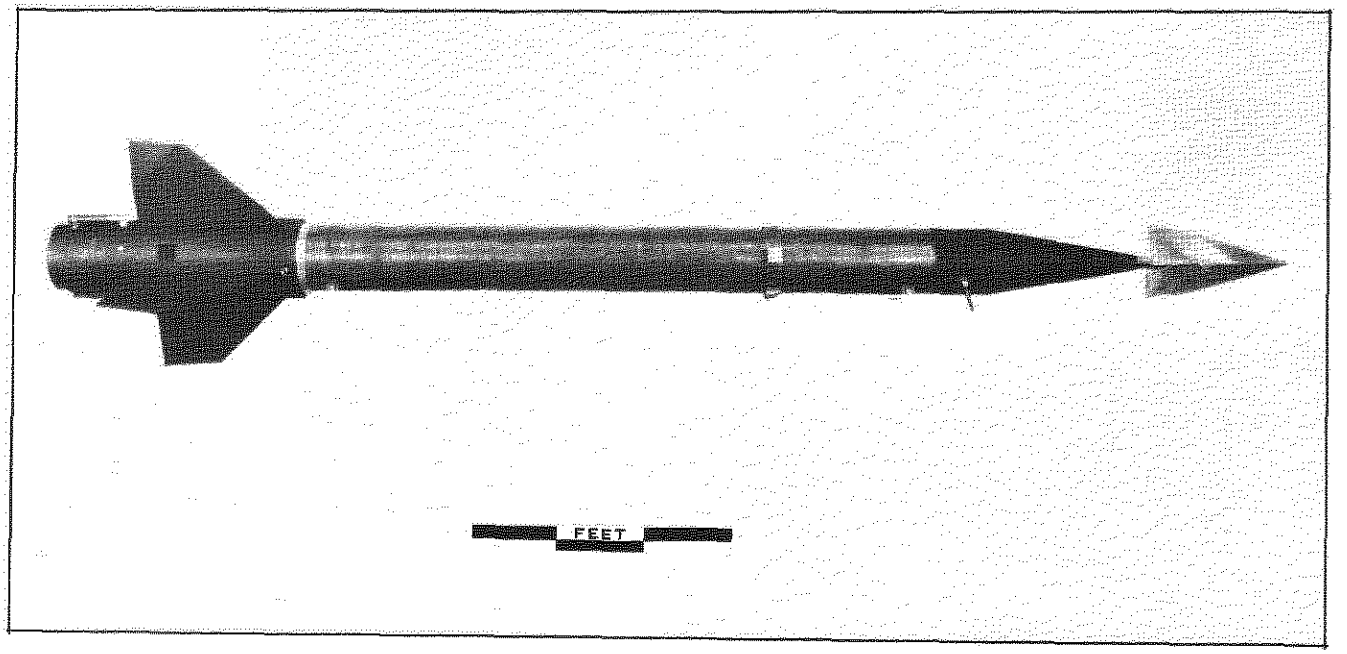

Fig.4b. Roll damping vehicle

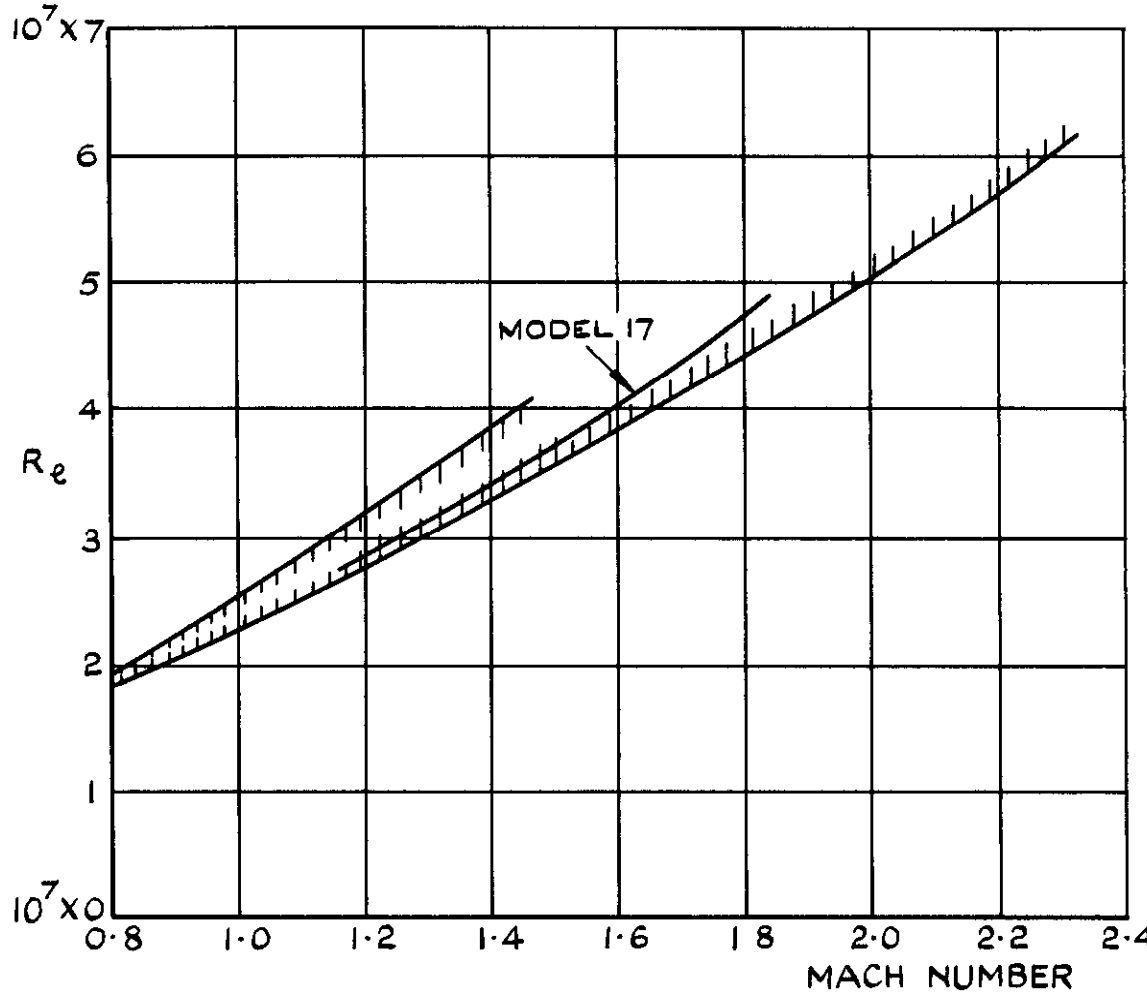

FIG. 5 REYNOLDS NUMBER (BASED ON $\bar{c}$)

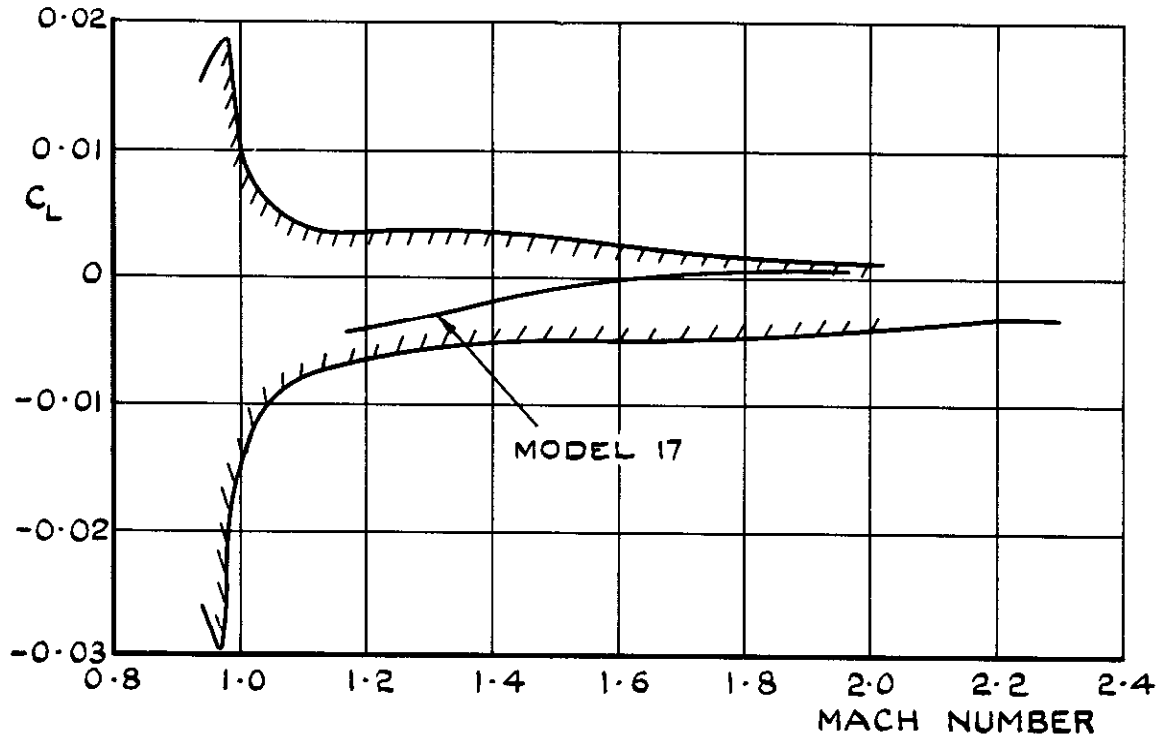

FIG. 6 (a) VARIATION OF LIFT – COEFFICIENT, C_L

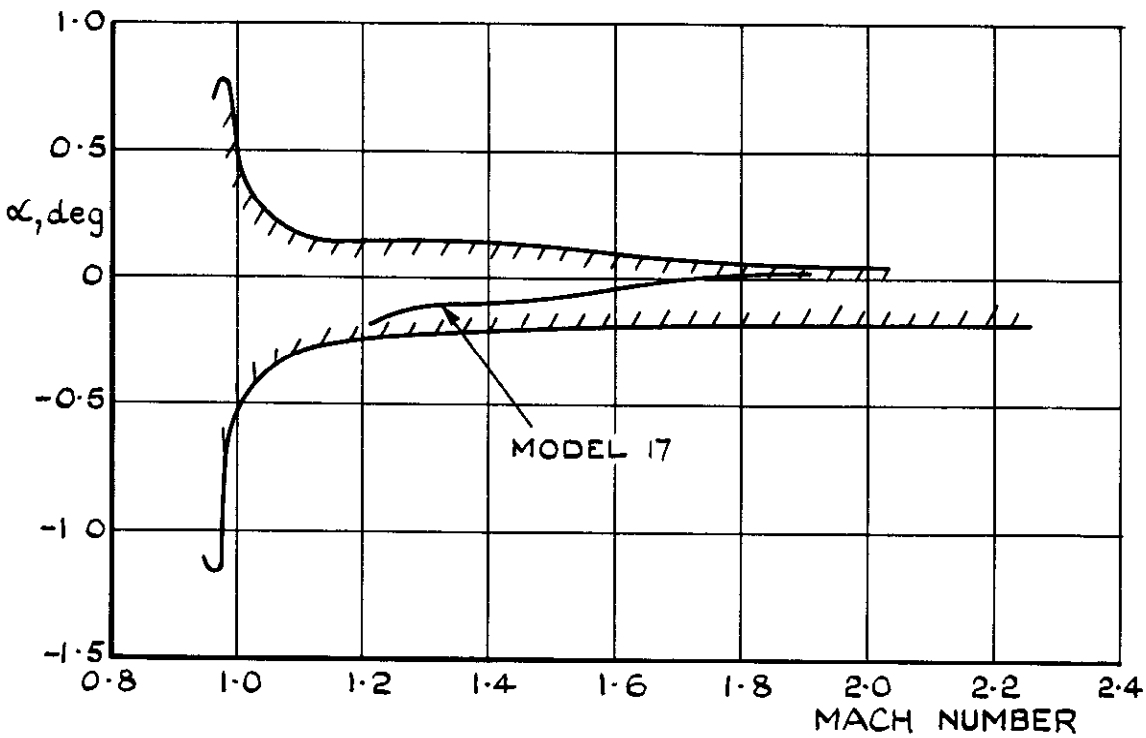

FIG. 6 (b) VARIATION OF INCIDENCE, α
(APPROXIMATE DERIVED VALUES)

FIG. 6 TRIM CONDITIONS

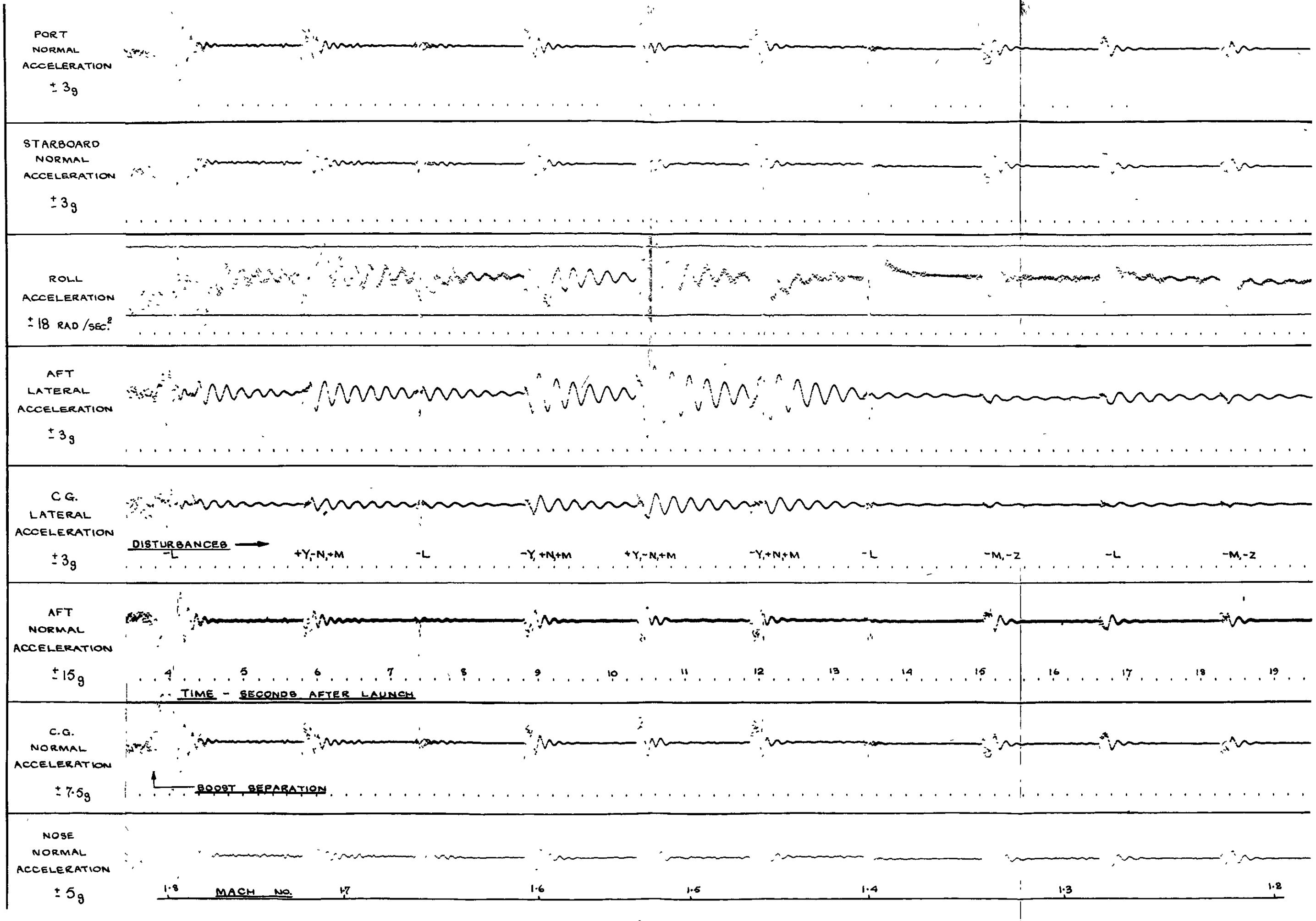

Fig.7 Telemetry record

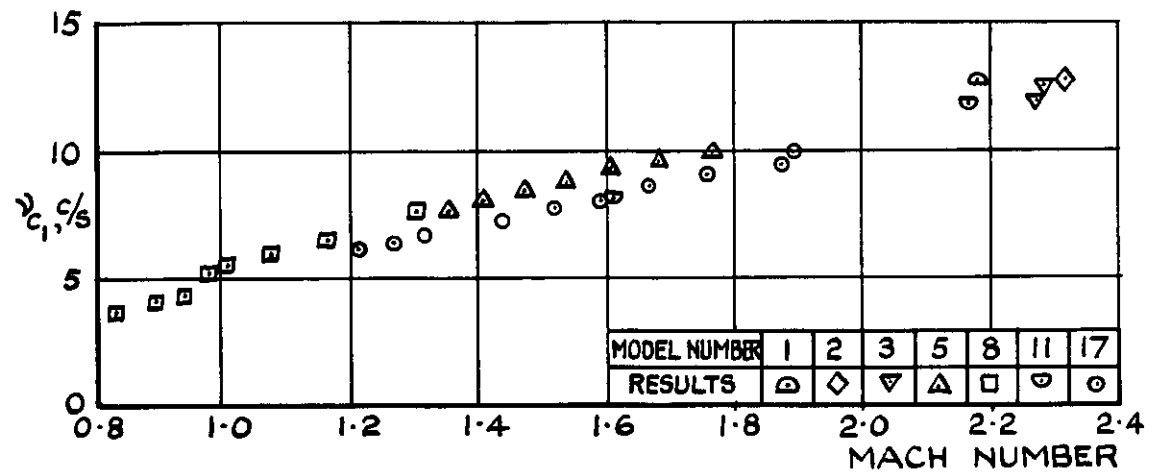

FIG. 8 (a) FREQUENCY OF SHORT-PERIOD LONGITUDINAL OSCILLATION.

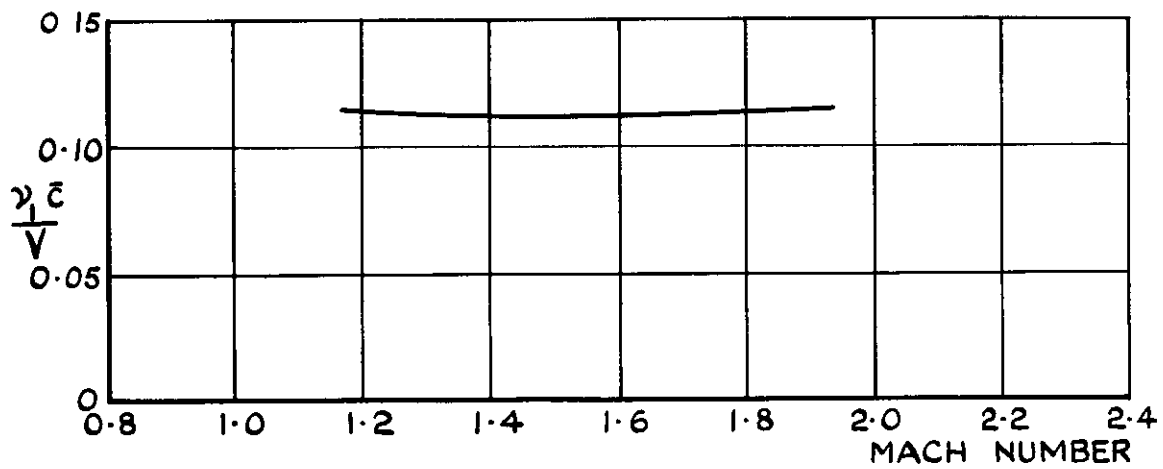

FIG. 8 (b) REDUCED FREQUENCY OF SHORT-PERIOD LONGITUDINAL OSCILLATION

FIG. 8 OSCILLATION FREQUENCIES

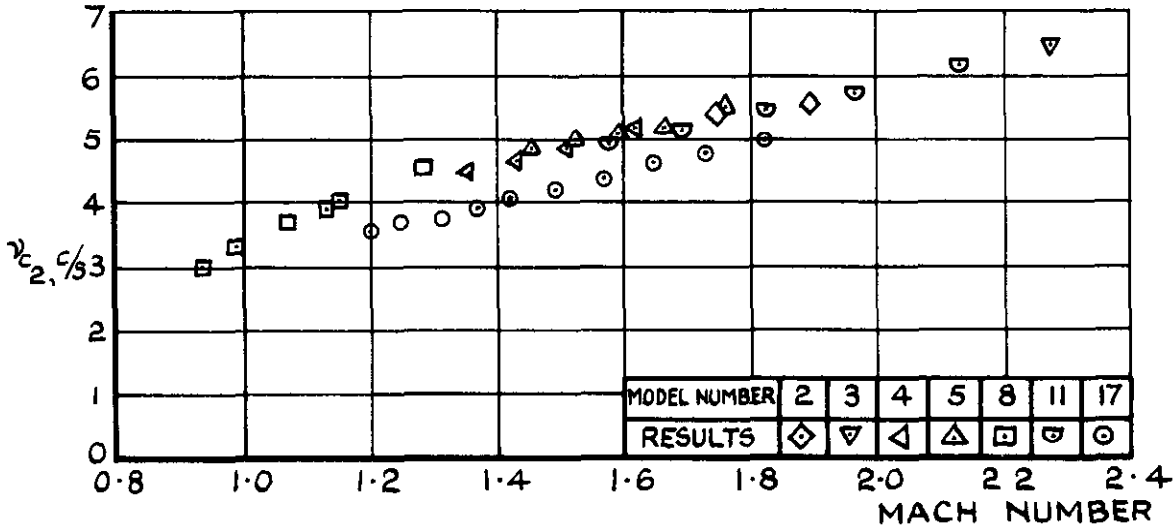

FIG.8 (c) FREQUENCY OF DUTCH-ROLL OSCILLATION

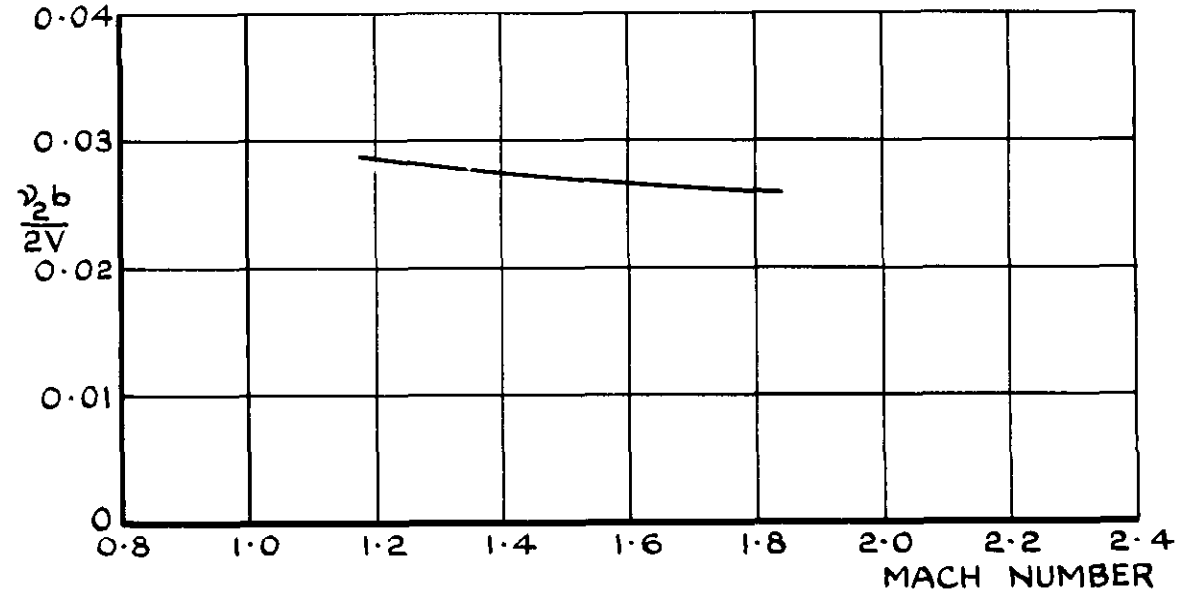

FIG.8 (d) REDUCED FREQUENCY OF DUTCH-ROLL OSCILLATION

FIG. 8 (CONT.) OSCILLATION FREQUENCIES

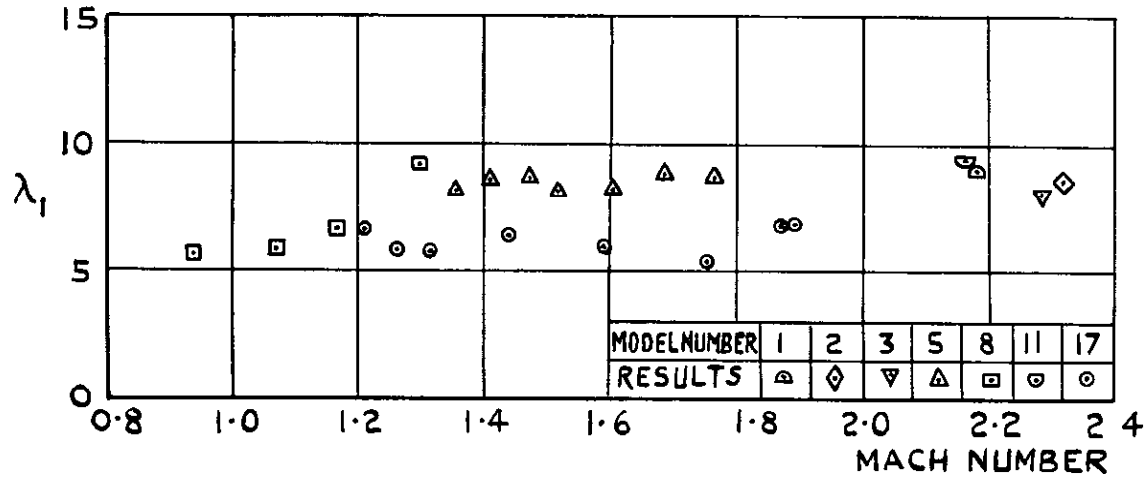

FIG.9 (a) TOTAL DAMPING OF SHORT-PERIOD LONGITUDINAL OSCILLATION

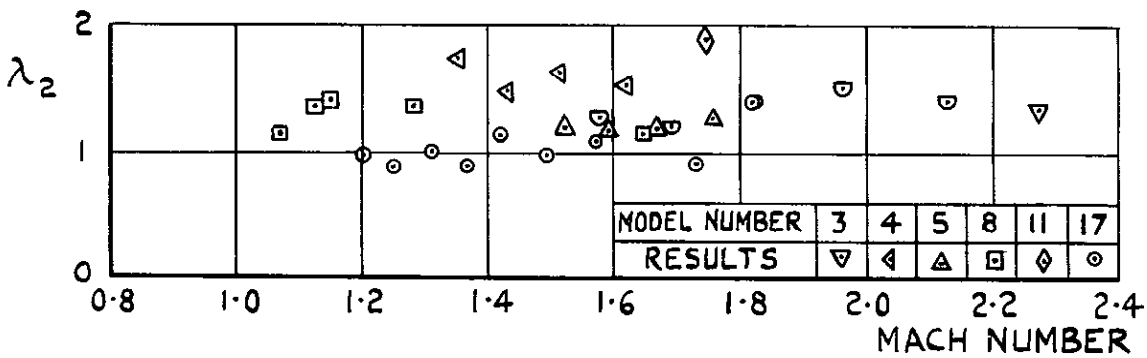

FIG.9 (b) TOTAL DAMPING OF DUTCH-ROLL OSCILLATION

FIG. 9 OSCILLATION DAMPINGS

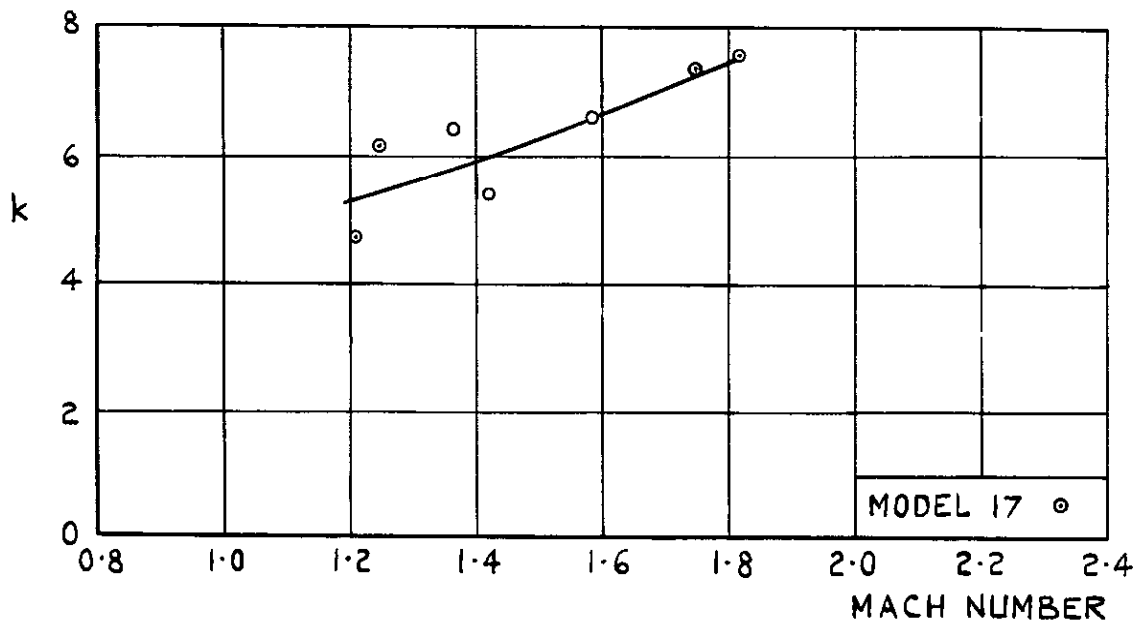

FIG.10 ROLL SUBSIDENCE DAMPING

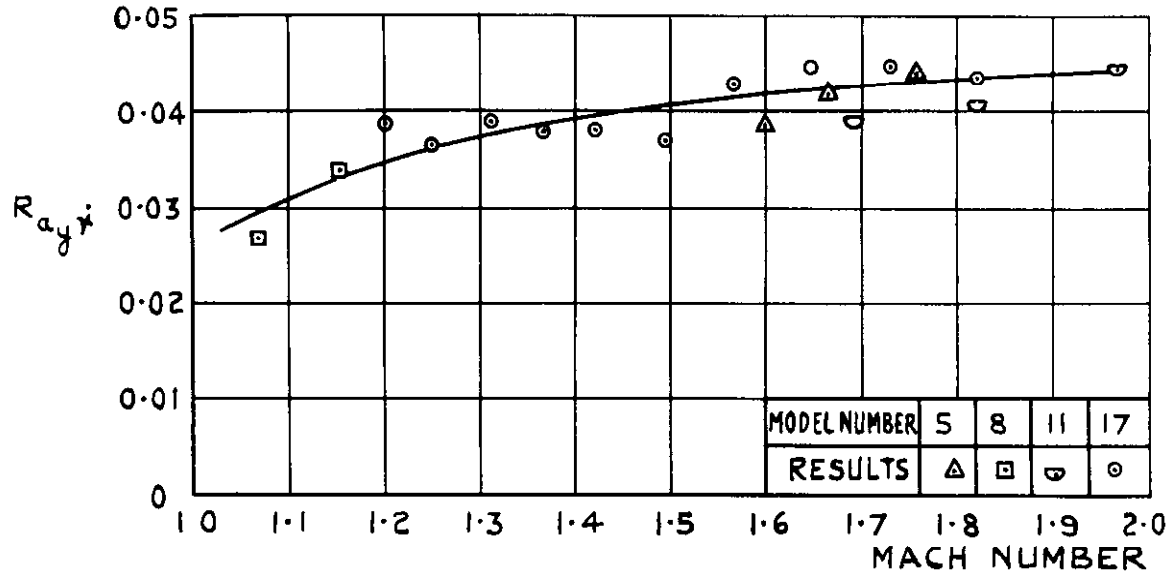

LATERAL ACCELERATION-YAW RATIO

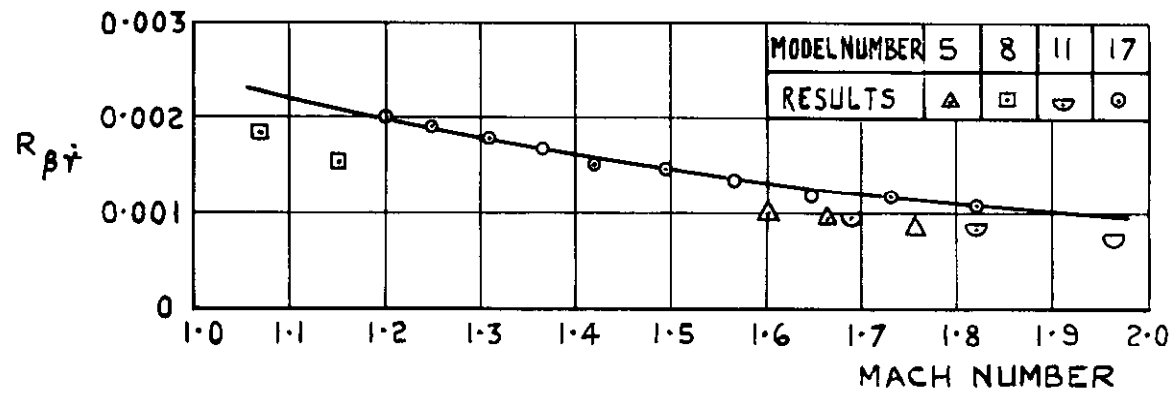

SIDESLIP-YAW RATIO

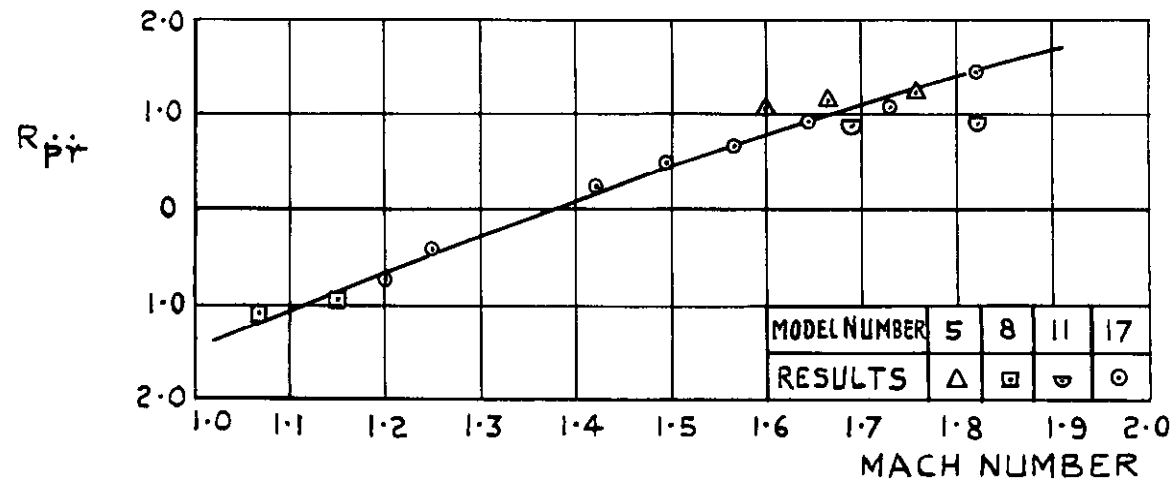

ROLL-YAW RATIO

FIG.11(a) AMPLITUDE RATIOS OF DUTCH-ROLL OSCILLATION

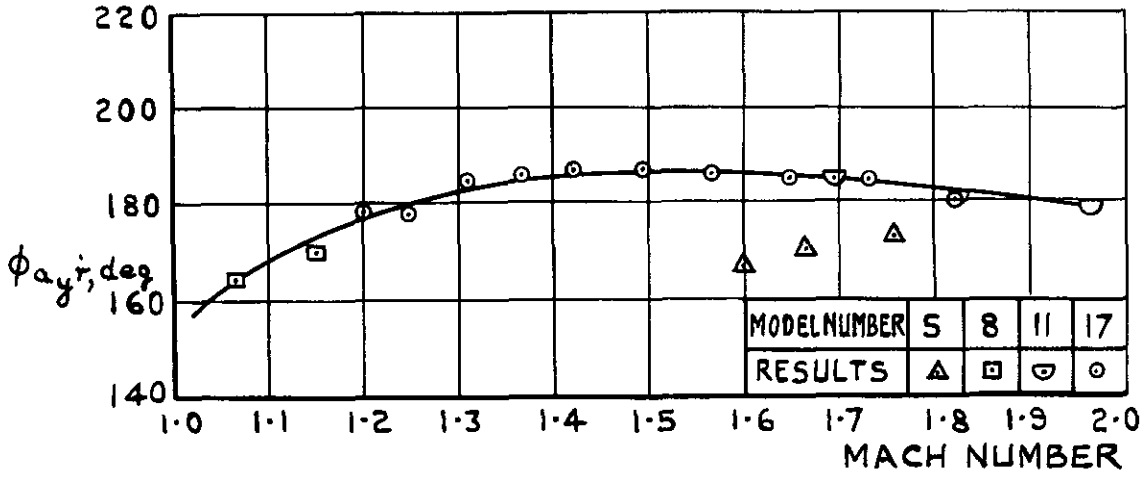

LATERAL ACCELERATION - YAW PHASE

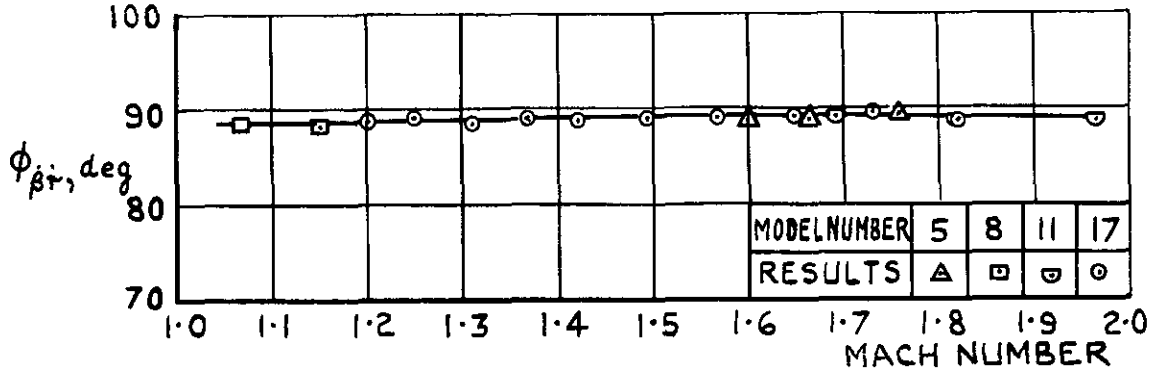

SIDESLIP - YAW PHASE

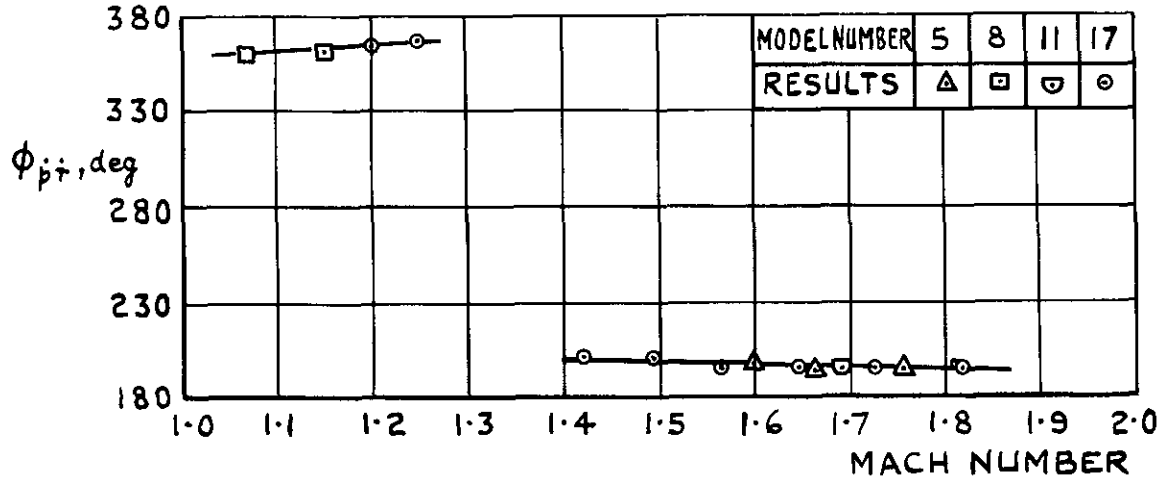

ROLL - YAW PHASE

FIG. 11(b) PHASE RELATIONSHIPS OF DUTCH-ROLL OSCILLATION

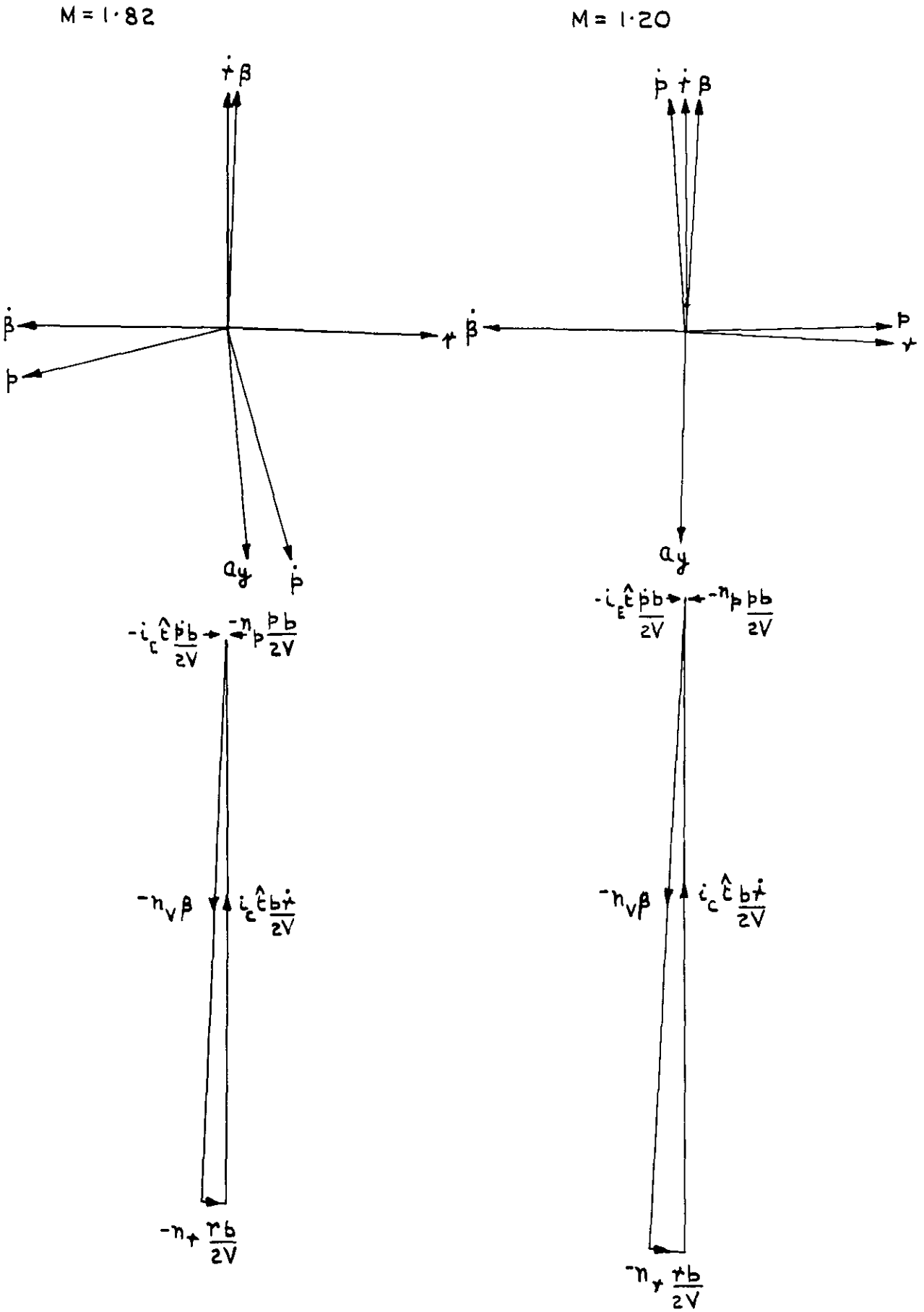

FIG. 12 (a) YAWING MOMENT EQUATION

FIG.12 VECTOR DIAGRAMS

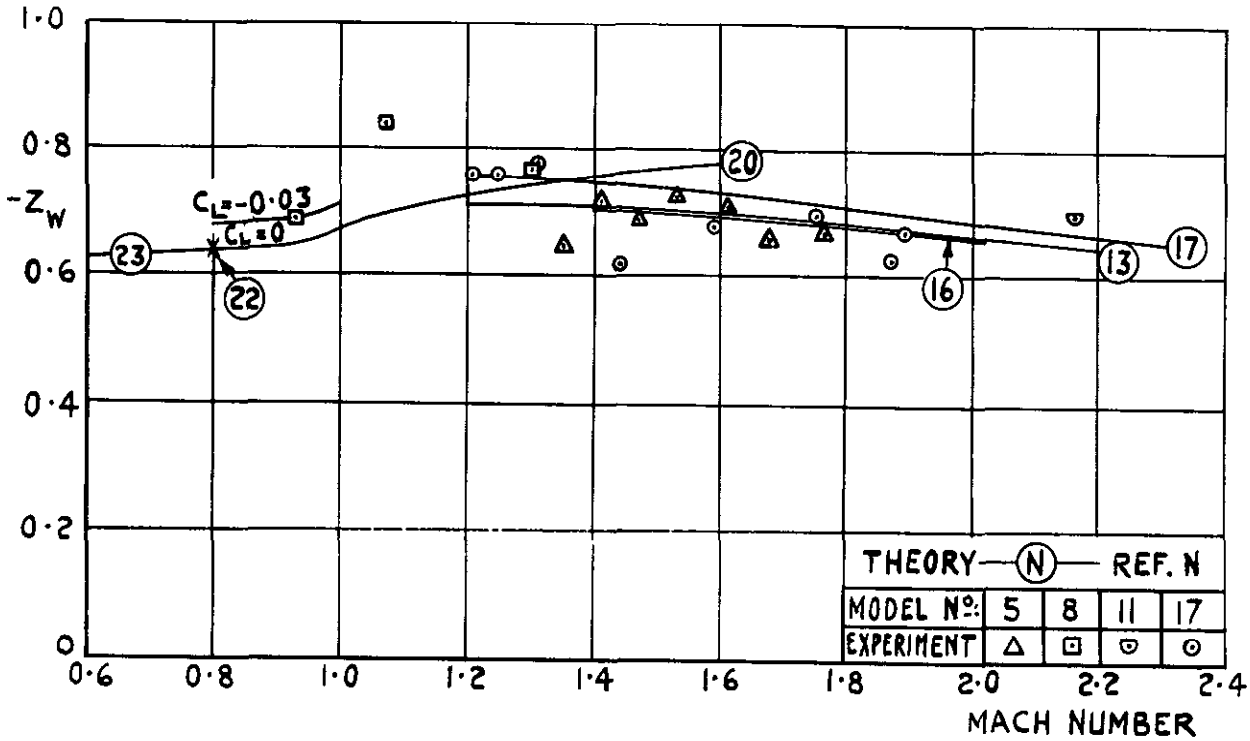

FIG.15 NORMAL FORCE DUE TO INCIDENCE, Z_w

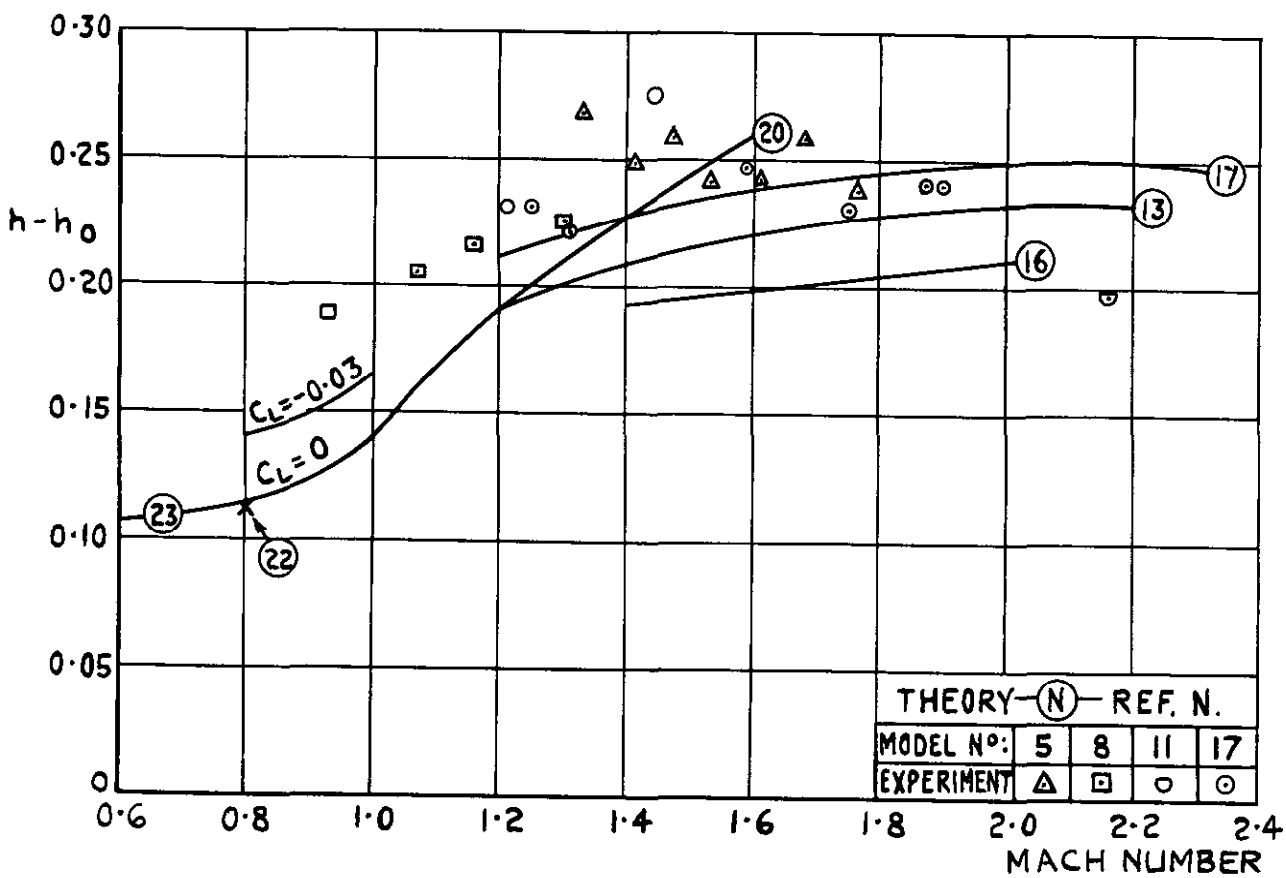

FIG.16 MANOEUVRE MARGIN, $h-h_o$

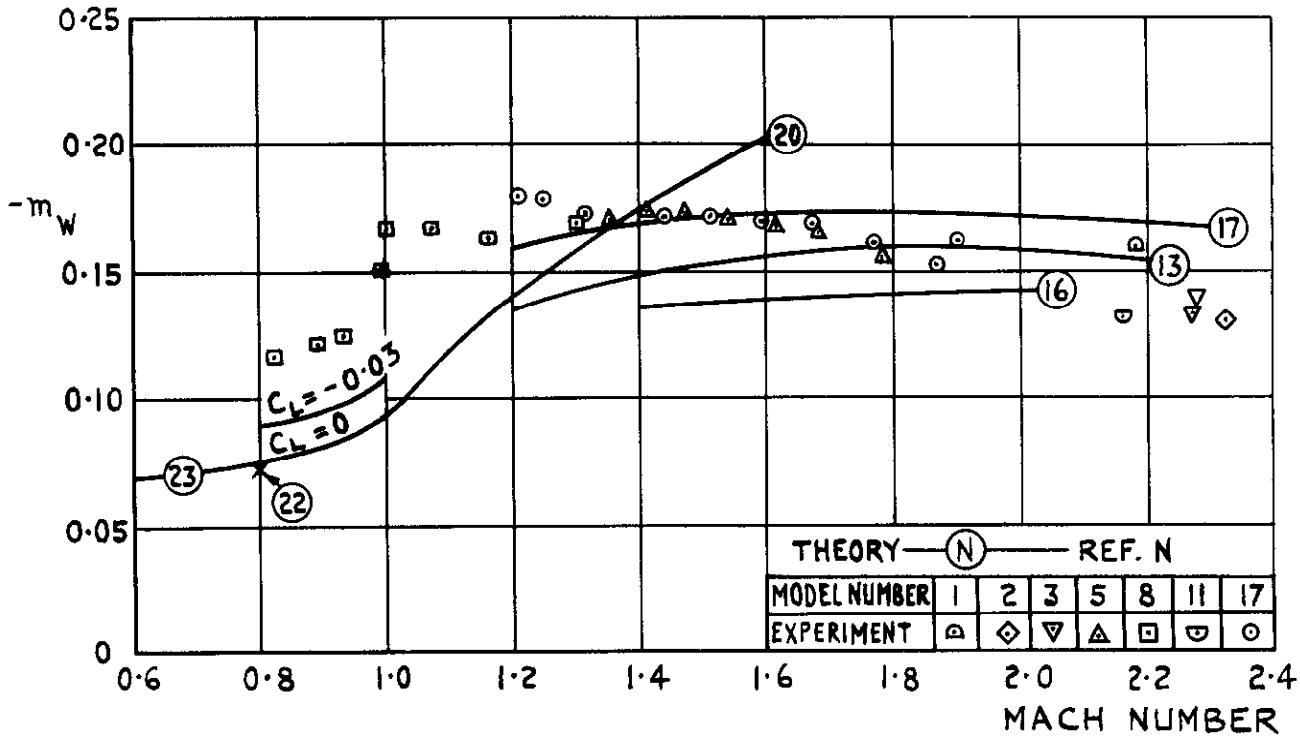

FIG.17 PITCHING MOMENT DUE TO INCIDENCE, m_w

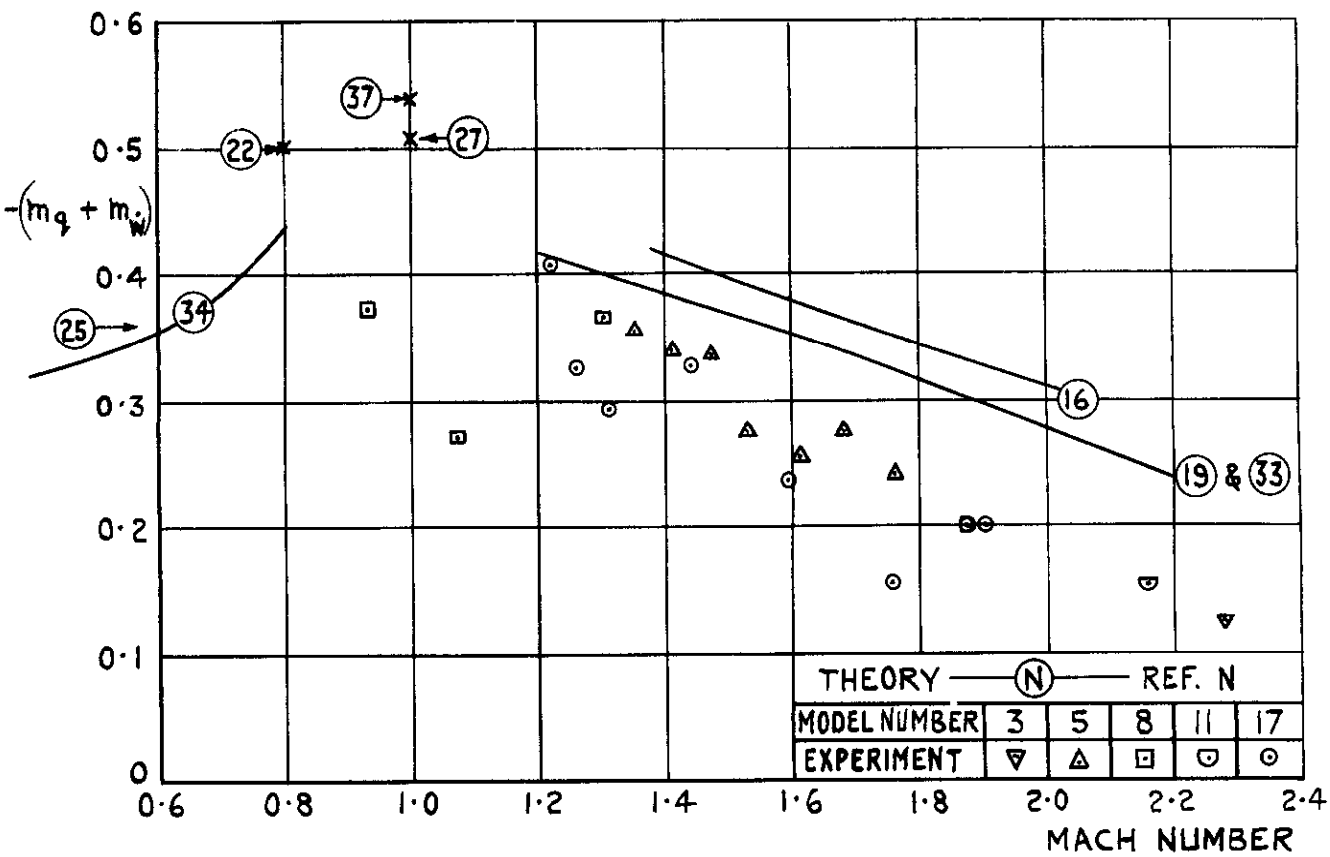

FIG.18 DAMPING-IN-PITCH DERIVATIVE, $m_q + m_{\dot{w}}$

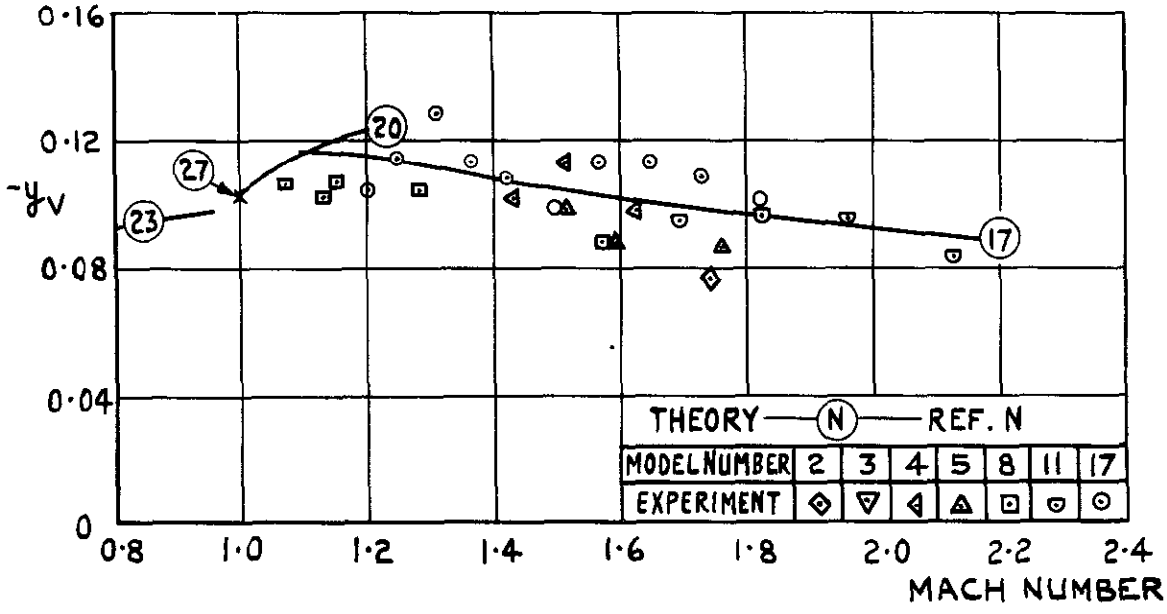

FIG. 19 SIDEFORCE DUE TO SIDESLIP, y_v

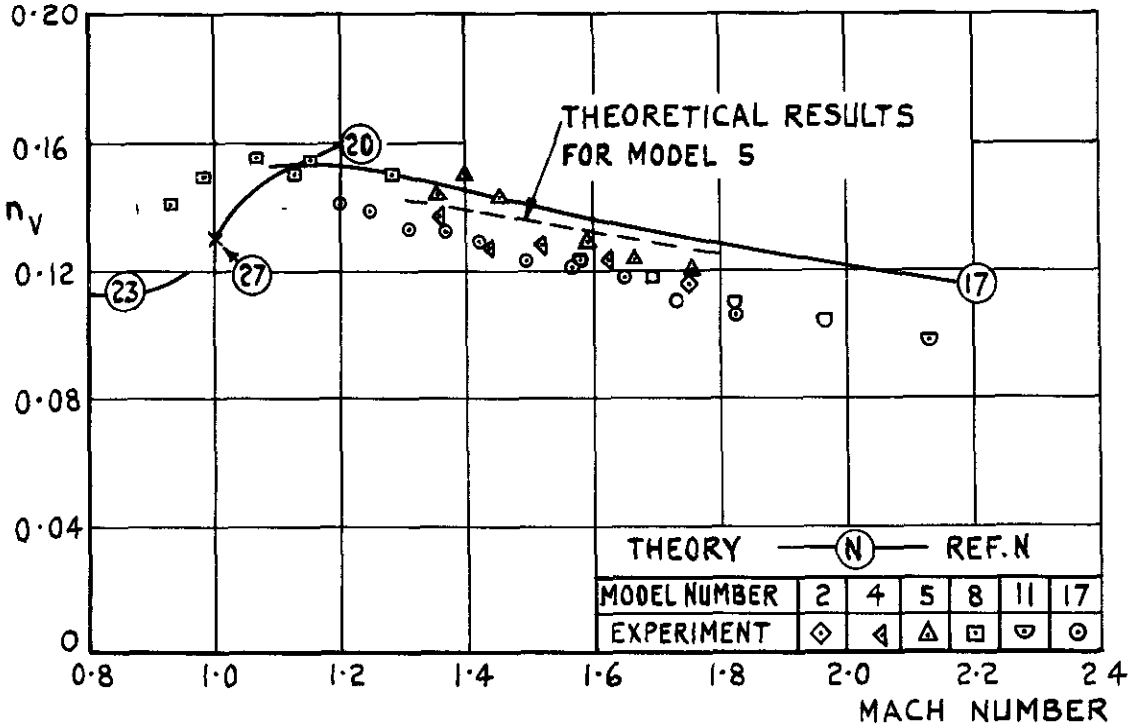

FIG. 20 YAWING MOMENT DUE TO SIDESLIP, n_v

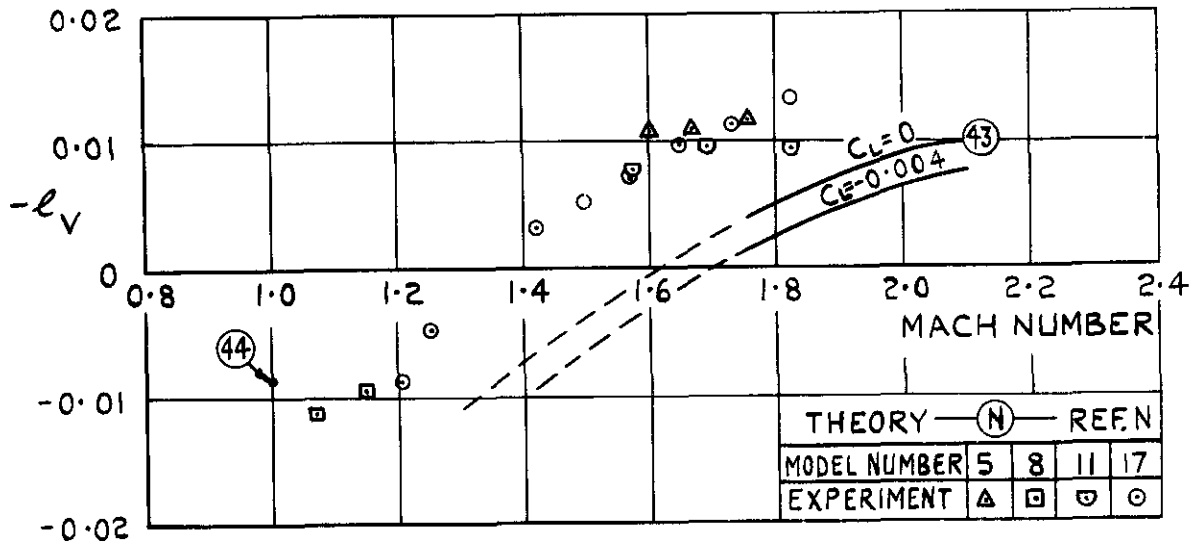

FIG. 21 (a) ROLLING MOMENT DUE TO SIDESLIP, ℓ_v

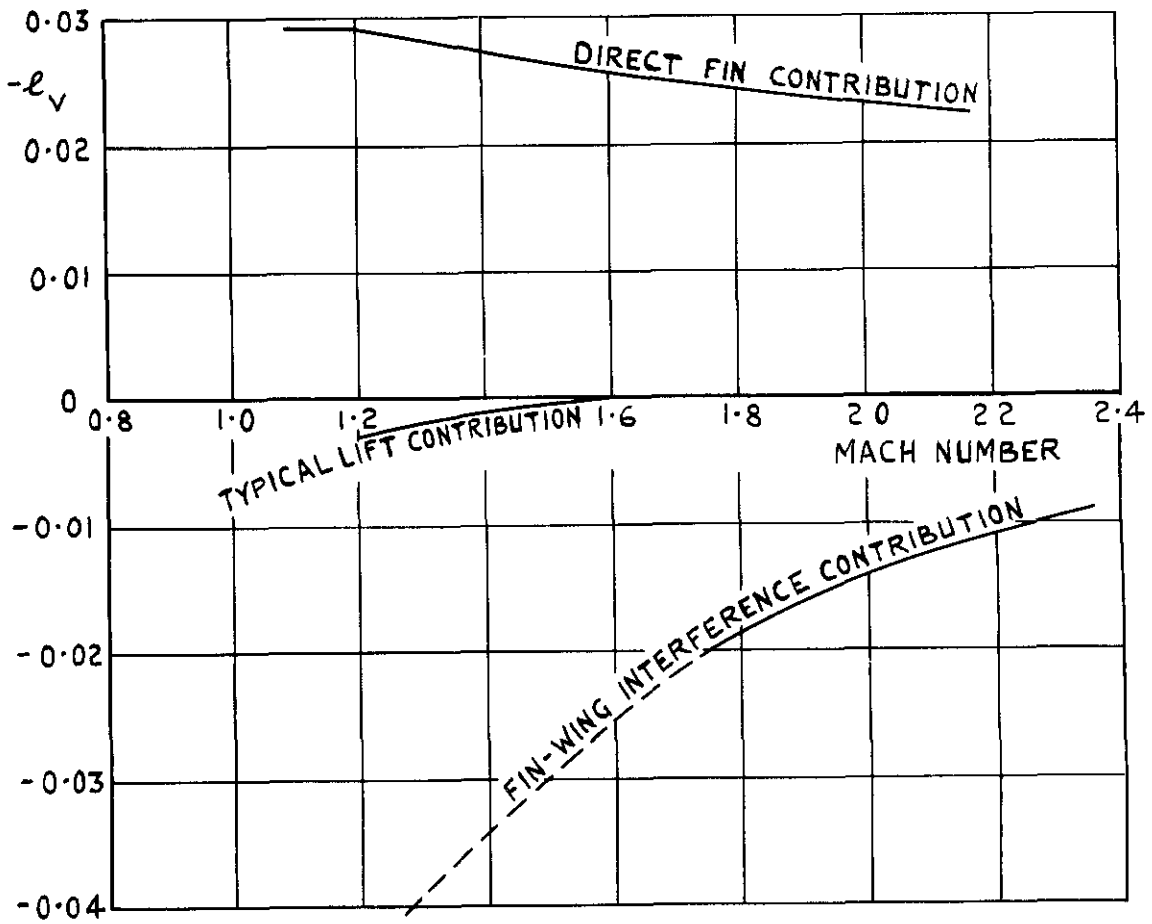

FIG. 21 (b) CONTRIBUTIONS TO ℓ_v

FIG. 21

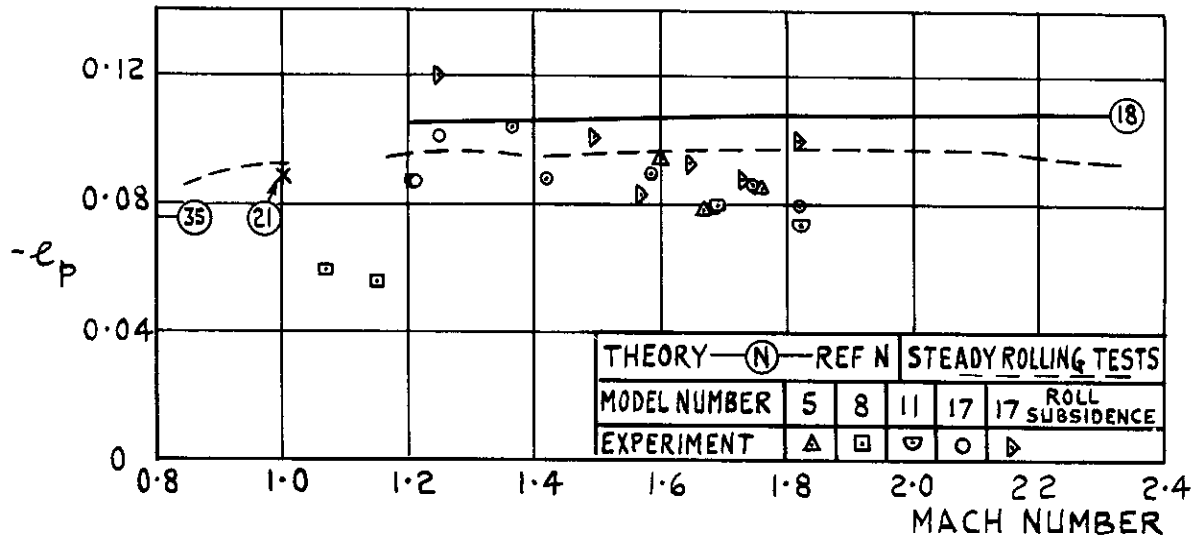

FIG. 22 (a) DAMPING-IN-ROLL DERIVATIVE, ℓ_p

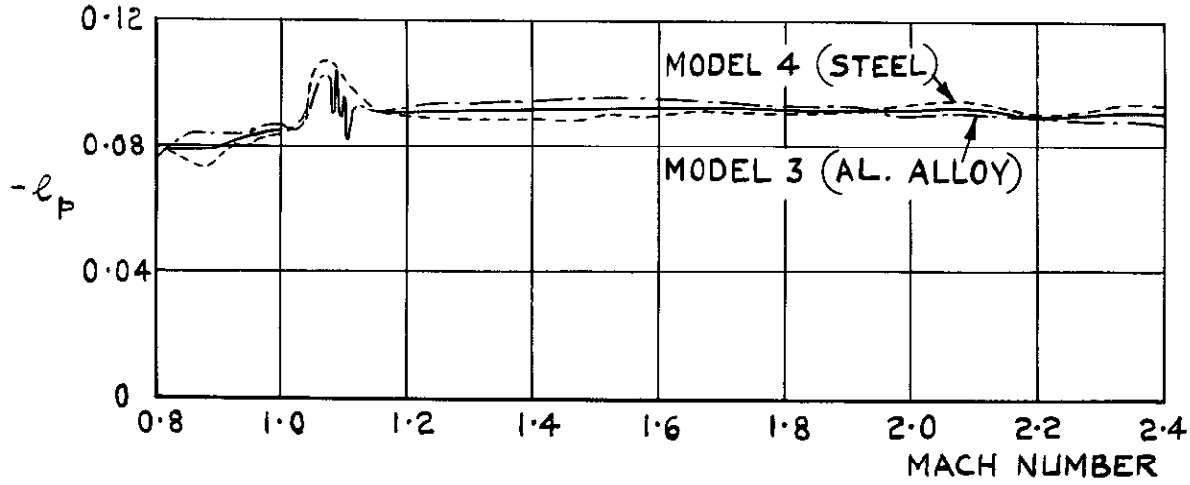

FIG. 22 (b) AERO-ELASTIC EFFECT ON ℓ_p

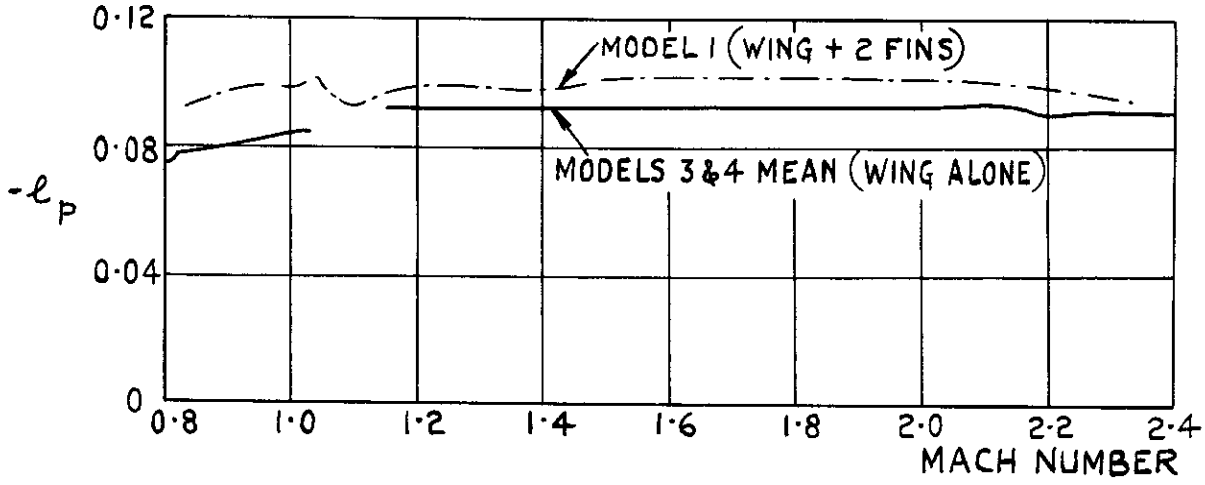

FIG. 22 (c) CONTRIBUTION TO ℓ_p FROM TWO FINS

FIG. 22

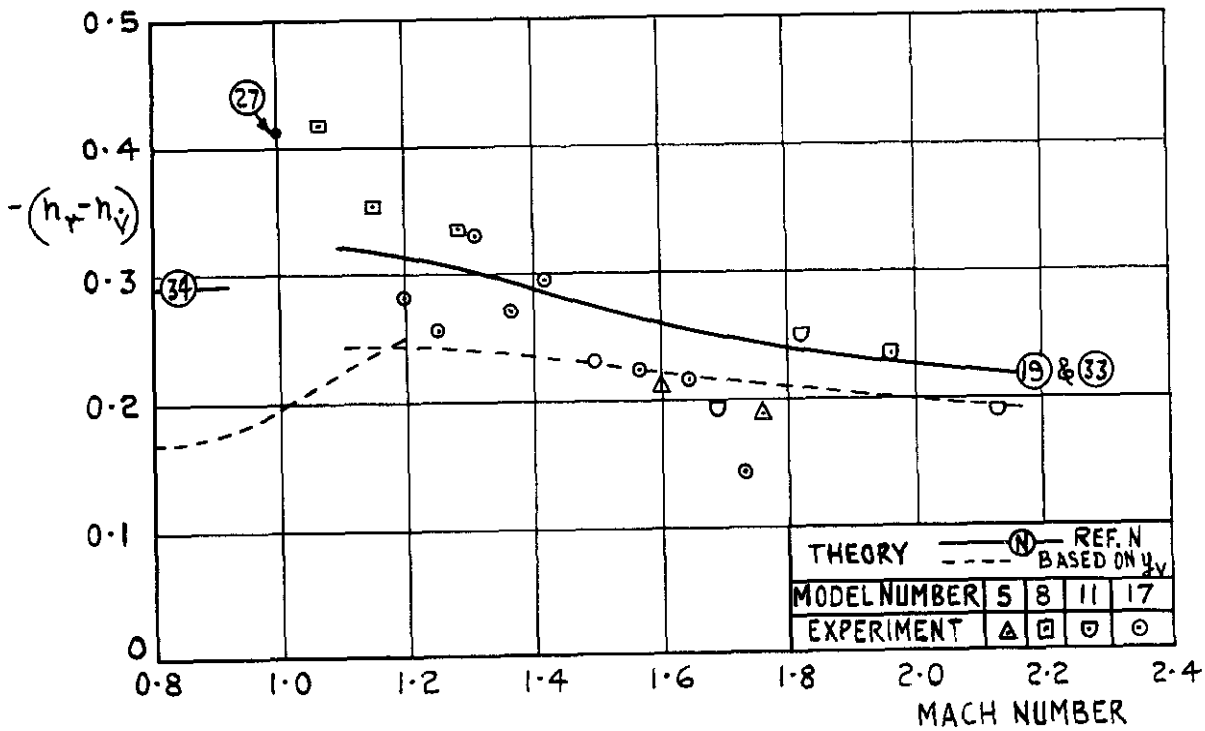

FIG. 23 DAMPING-IN-YAW DERIVATIVE, $n_r - n_{\dot{v}}$

Printed in England for Her Majesty's Stationery Office by the Royal Aircraft Establishment, Farnborough Dd 129528. K 3

A.R.C. C.P. No.995
June 1966

Turner, K.J.
Ross, A. Jean
Earley, Geraldine

533.6.013.417 :
533.693.3 .
533.6.011.34/5
533.6.072

THE DYNAMIC STABILITY DERIVATIVES OF A SLENDER WING, A COMPARISON OF THEORY WITH FREE-FLIGHT MODEL TESTS AT NEAR-ZERO LIFT, M - 0.8 to 2.4

Results are presented for the stability derivatives of a slender-wing and fin configuration as obtained from a series of tests with models flying at near-zero lift. These results are compared with theoretical estimates obtained from lifting surface theory at subsonic speeds and slender-wing and linearised supersonic theory at supersonic speeds. The agreement between the experimental and theoretical results is satisfactory, the largest discrepancies occurring at transonic speeds and at the higher supersonic Mach numbers.

A.R.C. C.P. No.995
June 1966

Turner, K.J.
Ross, A. Jean
Earley, Geraldine

533.6.013.417 :
533.693.3 :
533.6.011.34/5 :
533.6.072

THE DYNAMIC STABILITY DERIVATIVES OF A SLENDER WING, A COMPARISON OF THEORY WITH FREE-FLIGHT MODEL TESTS AT NEAR-ZERO LIFT, M = 0.8 to 2.4

Results are presented for the stability derivatives of a slender-wing and fin configuration as obtained from a series of tests with models flying at near-zero lift. These results are compared with theoretical estimates obtained from lifting surface theory at subsonic speeds and slender-wing and linearised supersonic theory at supersonic speeds. The agreement between the experimental and theoretical results is satisfactory, the largest discrepancies occurring at transonic speeds and at the higher supersonic Mach numbers.

A.R.C. C.P. No.995
June 1966

Turner, K.J.
Ross, A. Jean
Earley, Geraldine

533.6.013.417
533.693.3 .
533.6.011.34/5 .
533.6.072

THE DYNAMIC STABILITY DERIVATIVES OF A SLENDER WING, A COMPARISON OF THEORY WITH FREE-FLIGHT MODEL TESTS AT NEAR-ZERO LIFT, M = 0.8 to 2.4

Results are presented for the stability derivatives of a slender-wing and fin configuration as obtained from a series of tests with models flying at near-zero lift. These results are compared with theoretical estimates obtained from lifting surface theory at subsonic speeds and slender-wing and linearised supersonic theory at supersonic speeds. The agreement between the experimental and theoretical results is satisfactory, the largest discrepancies occurring at transonic speeds and at the higher supersonic Mach numbers.

DETACHABLE ABSTRACT CARDS

Published by
HER MAJESTY'S STATIONERY OFFICE

To be purchased from
49 High Holborn, London W C 1
423 Oxford Street, London W.1
13A Castle Street, Edinburgh 2
109 St Mary Street, Cardiff
Brazennose Street, Manchester 2
50 Fairfax Street, Bristol 1
258-259 Broad Street, Birmingham 1
7-11 Linenhall Street, Belfast 2
or through any bookseller

S.O. CODE No. 23-9017-95